Ab Initio Study of Hydrogen Abstraction Reactions

Harold Basch* and Shmaryahu Hoz

Department of Chemistry, Bar-Ilan University, Ramat Gan 52900, Israel

Received: December 17, 1996; In Final Form: March 26, 1997[⊗]

Ab initio electronic structure calculations have been carried out on six hydrogen abstraction reactions of the form, X−H + Y$^{\bullet}$ → X$^{\bullet}$ + H−Y, where X, Y = CH_3, NH_2, and OH. Geometric structures for the reactants, reactant complexes, transition states, product complexes, and products of each reaction have been gradient optimized at both the UMP2 and DFT(B3LYP) theory levels using the 6-311++G(2d,p) basis set. The character of each stationary state as a minimum or saddle point was determined by a harmonic force field calculation. PMP2 and CCSD(T) energies were also calculated at the UMP2 optimized geometries. CCSD(T) geometry optimizations were carried out for selected cases to resolve differences in results between UMP2 and DFT. The calculated reaction energies, barrier heights, and weak complex stabilities are compared to experiment, where possible, and among the different theory levels. The geometric structures and wave function properties are compared between the UMP2, CCSD(T), and DFT(B3LYP) methods. In general, all the methods predict reaction energies to within several kcal/mol of experiment. Calculated DFT(B3LYP) activation barriers are usually equal to or smaller than fitted Arrehenius equation activation energies (E_a), with the gap increasing as X and Y are more electronegative. The DFT(B3LYP) activation barrier for the CH_4 + $CH_3^{\bullet}$ reaction is, therefore, in the best agreement with experiment. The UMP2, PMP2//UMP2, and CCSD(T)//UMP2 methods give activation energies that are somewhat greater than E_a, as expected. The geometric structures of the three exchange reaction (X ≠ Y) transition states (TS) generally agree reasonably well between the UMP2 and DFT(B3LYP) methods, with active site bond length differences reflecting variations in the calculated exothermicities of the reactions. The UMP2 and DFT(B3LYP) methods give different conformations for the NH_3 + OH$^{\bullet}$ transition state, and CCSD(T) endorses the DFT results. For the H_2O + OH$^{\bullet}$ reaction UMP2 gives the symmetric structure as an energy minimum. DFT(B3LYP) predicts the symmetric structure to be the TS, in agreement with the optimized CCSD(T) result. For the NH_3 + $NH_2^{\bullet}$ reaction the UMP2 transition state is symmetric but with an unusually low imaginary reaction path frequency, while the DFT(B3LYP) frequency is reasonable. CCSD(T)//UMP2 and DFT(B3LYP) hydrogen-bonding energies for the reaction and product complexes are very similar and generally smaller than the UMP2 and PMP2//UMP2 results. The equilibrium geometric structures at the UMP2 and DFT(B3LYP) levels generally agree reasonably well. However, for the NH_2···H−OH product complex DFT(B3LYP) gives a planar conformation, while UMP2 predicts a C_s nonplanar configuration.

1. Introduction

Chemists have been in search of practical tools for the theoretical studies of chemical reactions since the inception of quantum mechanics. Recent advances in methodology and developments in computer technology have combined to make high-level *ab initio* calculations on the reaction paths of elementary reactions in the gas phase feasible.[1] A very popular *ab initio* correlation method is second-order Moller−Plesset (MP2)[2,3] perturbation theory. The unrestricted HF (UHF) wave function forms the basis for the UMP2 description. Unfortunately, the UHF wave function is not necessarily or generally an eigenfunction of the spin-squared ($\mathbf{S}^2$) operator, and its expectation value ($\langle \mathbf{S}^2 \rangle$) can be far from the theoretically exact $S(S=1)$, where S is the desired spin state of the wave function. In such cases, the shape of a calculated energy surface and the location of the stationary states can be adversely affected.[4,5] Spin projection to annihilate the major spin contaminant(s) has been proposed to give the PUMP2 method (PMP2 for short) with a $\langle \mathbf{S}^2 \rangle$ value that is much closer to exact than UMP2. PMP2 often gives better agreement with the results of more rigorous theory levels.[6−9] One of the more accurate model levels is coupled cluster theory,[10] including a noniterative addition of triple excitations, CCSD(T).[11] This scheme gives results that have been shown to be relatively stable with regard to modest spin contamination in the unrestricted case.[9,12]

Density functional theory (DFT)[13,14] using gradient-corrected exchange and correlation potentials (generically called the generalized gradient approximation, GGA[15]) has been shown to be a useful and accurate tool in computing geometric structures, vibrational frequencies, and even bond dissociation energies.[13,16] Mixing in an amount of the "exact" HF exchange, to give what are called hybrid functionals, improves performance for a variety of properties.[17,18] The unrestricted DFT wave function is typically much less spin contaminated than the corresponding UHF wave function for a given open shell system.[19] The most often quoted comparable level of accuracy to DFT for closed shell molecules is the MP2 level.[14] Such a determination has not yet been made for radical systems. The hybrid functional in DFT seems to perform better than GGA methods because of a cancellation of errors due to spurious self-interaction in DFT and the neglect of correlation in HF.[20] This seems to be especially important for describing bonds involving hydrogen atoms.[21] A number of studies of transition state properties by density functional theory have been carried out[20,22−35] assessing its performance by comparison to experi-

[⊗] Abstract published in *Advance ACS Abstracts,* May 15, 1997.

S1089-5639(97)00011-X CCC: $14.00

ment and to other theoretical methods. The results have been erratic.

The modeling of reaction kinetics is important for scientific and technological needs. Typical reaction processes involve many elementary intermediate, sequential, or simultaneous reaction steps, and the energetics and kinetics of each elementary reaction are needed in order to model the overall reaction process.[36] Most such reactions involve free radical addition or transfer. Although the actual chemical reaction rate results from the dynamical motion of all the relevant species on the potential energy surface, the kinetic constant of each elementary step can be estimated from rate theories if the barrier height, structure, and vibrational frequencies of the transition state (TS) connecting reactants and products are known.[37a] Further, although problematic, empirical relations between structure−reactivity parameters and the electronic and geometric structural nature of the TS are routinely used by physical organic chemists to draw conclusions about the factors that govern chemical reactivity.[37b] Therefore, a great deal of effort has been invested in determining the location, structure, and energy of transition states,[38] by *ab initio*,[5] semiempirical,[39a] and empirical[39b] methods. Evaluating the accuracy of calculated TS properties is difficult since the TS is not usually amenable to direct experimental study. It is, therefore, useful to calibrate the different theoretical methods used to calculate transition states against each other. In addition, the database of studied reaction paths should be constantly expanded, both to provide new information and to widen the range of tests and comparisons that can be used to validate the different theory levels.

In this work we have carried out MP2, CCSD(T), and DFT(B3LYP) calculations to determine the stationary points for the following set of six hydrogen abstraction or transfer reactions:

$$CH_4 + CH_3^\bullet \rightarrow CH_3^\bullet + CH_4 \quad (1)$$

$$CH_4 + NH_2^\bullet \rightarrow CH_3^\bullet + NH_3 \quad (2)$$

$$CH_4 + OH^\bullet \rightarrow CH_3^\bullet + H_2O \quad (3)$$

$$NH_3 + NH_2^\bullet \rightarrow NH_2^\bullet + NH_3 \quad (4)$$

$$NH_3 + OH^\bullet \rightarrow NH_2^\bullet + H_2O \quad (5)$$

$$H_2O + OH^\bullet \rightarrow OH^\bullet + H_2O \quad (6)$$

These reactions proceed, presumably, by the concerted breaking of the old (X−H) bond and the making of the new (H−Y) bond. In such reactions, the reactants (R) can often form a weakly bound complex (RC) before proceeding to the TS, which then breaks up to form a weakly bound product complex (PC) before proceeding to the asymptotic products (P):

$$R \rightarrow RC \rightarrow TS \rightarrow PC \rightarrow P \quad (7)$$

The hydrogen abstraction reactions studied here are represented generically as

$$X{-}H + Y^\bullet \rightarrow X^\bullet + H{-}Y \quad (8)$$

where X and Y can each be CH_3, NH_2, or OH. These combinations of X and Y groups give rise to three symmetric or identity (X = Y) and three nonsymmetric or exchange (X ≠ Y) reactions. All of these reactions have been studied previously by one group,[40] but at lower levels of *ab initio* theory that did not include DFT and did not locate reaction and product complexes. These types of hydrogen abstraction reactions are major players in fuel combustion, oxidation, and atmospheric processes involving hydrocarbons (like methane), ammonia, and the ubiquitous hydroxyl radical.

The energy properties examined here include heats of reaction, where nonzero, transition state barrier heights, and the stabilities of reaction and product complexes. The latter are expected to generally look like X−H···Y and X···H−Y, respectively. However, each such complex geometry may not be a global minimum on the potential energy surface, either in the entrance channel for the reactants or in the exit channel for the products. An additional complication is offered by the possibility of weak complex formation with different spatial orientations of the unpaired spin, corresponding to complexes with different electronic states. These different possible geometric structures, including those for the transition state, offer a wide variety of geometry types that can provide a sensitive comparison of different theoretical methods.

2. Methods

All of the calculations reported here were carried out using the Gaussian 94 set of programs.[41] Therefore, the composite B3LYP functional used here in the DFT method is taken from the specific hybrid combination of exchange and correlation density functionals, and Hartree−Fock exchange defined by Frisch.[42] Cross reactions 2, 3, and 5 are written in the exothermic direction. Geometric structures for the R, RC, TS, PC, and P type species (eq 7) in reactions 1−6 were gradient optimized with no symmetry constraints at both the UMP2 (frozen core) and unrestricted DFT(B3LYP) theory levels. In both cases the standard 6-311++G(2d,p) basis set was used with six d-type components. The nature of each stationary point was established by a harmonic force field frequency calculation using analytical energy second derivatives. The number of imaginary frequencies determines the type of stationary point: 0 for a minimum energy structure and 1 for a saddle point. The vibrational frequency calculation also supplies the zero-point energy (ZPE) of each structure and room temperature translational, rotational, and vibrational thermal corrections to the total electronic energy.[3] These were obtained separately at the UMP2 and DFT(B3LYP) levels and applied to the electronic energy differences, where indicated, without any scaling factor. Spin-projected UMP2 (PMP2) energies were also calculated at the UMP2 optimized geometries [PMP2//UMP2] for each of the radical species, following the spin projection method of Schlegel.[9] The extent to which the PMP2 and UMP2 energies differ is an indication of the importance of correcting for spin contamination in the calculated electronic energy values.

Single-point CCSD(T) energies were also calculated at the optimized UMP2 structures using the same 6-311++G(2d,p) basis set [CCSD(T)//UMP2]. UCCSD(T) was used for the radical species. The ZP+thermal (T = 298 K) energy corrections obtained at the UMP2 level were used also for the PMP2 and CCSD(T) energies, where indicated. For each UMP2 transition state the intrinsic reaction coordinate (IRC)[43] was generated pointwise on the reaction path on both the reactant and product sides of the TS. For the asymmetric abstraction reactions CCSD(T) energies were calculated at the UMP2 IRC points surrounding the TS to find a new interpolated extremum. For the symmetric reactions the X···H distances were CCSD(T) optimized in a pointwise fashion. These procedures give a rough approximation to a CCSD(T) optimized geometric structure for the transition state.[44] For the transition states of the $H_2O + OH^\bullet$ and $NH_3 + OH^\bullet$ reactions where a qualitative difference in optimum geometric configuration or structure was

TABLE 1: Energies of the Stationary States in the X−H + Y• → X• + H−Y Reaction[a]

X	Y	struct	UMP2	PMP2//UMP2	CCSD(T)//UMP2	DFT(B3LYP)
CH_3	CH_3	R	−80.105 994	−80.107 886	−80.158 366	−80.392 054
(Figure 1)[b]		RC′	−80.106 425	−80.108 361	−80.158 885	
		RC(**1**)	−80.106 563	−80.108 491	−80.159 017	
		TS(**1**)	−80.074 588	−80.079 953	−80.128 541	−80.367 181
					−80.128 643[c]	
CH_3	NH_2	R	−96.139 103	−96.141 068	−96.188 478	−96.438 077
(Figure 2)[b]		RC(**2**)	−96.140 465	−96.142 424	−96.189 878	−96.438 711
		TS(**2**)	−96.114 057	−96.120 041	−96.163 400	−96.420 255
					−96.163 249[d]	
		PC(**2**)	−96.147 639	−96.149 537	−96.192 417	−96.442 787
		PC′(**2**)	−96.146 783	−96.148 705	−96.191 574	−96.442 043
		P	−96.145 402	−96.147 330	−96.190 130	−96.441 183
CH_3	OH	R	−115.986 347	−115.988 159	−116.030 778	−116.299 446
(Figure 3)[b]		RC′				−116.299 966
		RC(**3**)	−115.987 708	−115.989 509	−116.032 141	−116.300 200
		TS(**3**)	−115.970 548	−115.975 662	−116.017 068	−116.295 577
					−116.016 920[d]	
		PC(**3**)	−115.011 835	−115.013 730	−116.049 014	−116.319 267
		P	−116.009 405	−116.011 333	−116.046 564	−116.316 941
NH_2	NH_2	R	−112.178 547	−112.180 512	−112.220 242	−112.487 202
(Figure 4)[b]		RC′(**4**)	−112.184 745	−112.186 675	−112.226 291	−112.492 943
		RC(**4**)	−112.183 186	−112.185 148	−112.224 780	−112.490 990
		TS(**4**)	−112.157 443	−112.164 437	−112.200 268	−112.477 028
					−112.200 511[c]	
NH_2	OH	R	−132.025 791	−132.027 603	−132.062 542	−132.348 571
(Figure 5)[b]		RC(**5**)				132.356 884
		RC′(**5**)	−132.038 563	−132.040 326	−132.074 973	−132.361 782
		TS(**5**)	−132.011 670[g]	−132.016 887	−132.053 737	−132.352 920[h]
					−132.053 584[d]	
		PC(**5**)	−132.051 413[g]	−132.053 393	−132.085 251	−132.371 405[h]
		P	−132.042 550	−132.044 515	−132.076 676	−132.362 960
OH	OH	R	−151.889 794	−151.891 606	−151.918 976	−152.224 329
(Figure 6)[b]		RC(**6**)	−151.895 706	−151.897 525	−151.924 855	
		RC′(**6**)	−151.900 007	−151.901 772	−151.928945	−152.234 387
		TS(**6**)[e]	−151.870 601	−151.876 959	−151.903 377	
		SS(**6**)[f]	−151.871 115	−151.879 085	−151.902 552	−152.222 257
					−151.902 719[c]	

[a] Energy in au. [b] Figure numbers in parentheses. [c] One-dimensional symmetric X···H distance CCSD(T) optimization. [d] One-dimensional optimization using the UMP2 IRC geometries about the TS. [e] Asymmetric TS. [f] Symmetric structure; TS(DFT) or minimum(UMP2). [g] Structure a in Figure 5. [h] Structure b in Figure 5.

found between the UMP2 and DFT(B3LYP) methods, a numerical CCSD(T) geometry optimization was also carried out in the same 6-311++G(2d,p) basis set to distinguish between the competing structures.

It should be noted that the potential energy surfaces of the reaction and product complexes are very flat, with concomitant difficulties in convergence to stationary points in the geometry optimization. The large number of diffuse functions in the 6-311++G(2d,p) basis set could also contribute to convergence difficulties, which were sometimes encountered also at the SCF level. Because the OH and NH_2 radicals have both Σ and Π symmetry low-lying spin doublet electronic states, it sometimes happens that the SCF procedure locks into an excited state or into the upper branch of a symmetry split Π state (OH). This can also cause SCF convergence difficulties. Problems of electronic state identity were usually handled by carefully preparing the initial electronic configuration. The reaction and product complexes were pre-positioned in their least motion path or hydrogen-bonded positions, or taken from asymptotic IRC geometries. As indicated in the individual cases, in the course of the gradient geometry optimization these initial structures sometimes rotated to give a more stable conformer, or even dissociated. Therefore, not every corresponding type of reaction and product complex was found at both the UMP2 and DFT(B3LYP) theory levels. When the UMP2 and DFT methods gave different equilibrium geometry complexes or transition states, the geometries were switched between them and reoptimized to ascertain the true extremum point structure at each theory level.

3. Results and Discussion

The numerical results are presented in Tables 1−7. Table 1 summarizes the calculated total electronic energies of the stationary points for each reaction. The energy differences are summarized in Table 2, together with experimental results, where known. Those calculated energy differences that can be compared directly with experimental data have been corrected for ZPE+thermal (T = 298 K) energy effects in the usual manner.[3] The energies have not been corrected for basis set superposition error (BSSE).[45] In any event, the DFT(B3LYP) binding energies should have a smaller BSSE contribution than the UMP2 values since in the latter case the excited state summation is usually a significantly larger source of BSSE than the SCF level.[46] For the same structures then, the calculated binding energies of the weakly bound complexes are expected to be larger at the UMP2 level than the DFT level. On the other hand, some of these complexes have structures with long intermolecular equilibrium distances and very low binding energies that correspond more to van der Waals interactions than to the normal hydrogen-bonded geometries expected on these reaction paths. DFT methods behave erratically in describing dispersion forces and the hybrid functionals have been found to underestimate such interactions.[47]

Table 3 presents the calculated $\langle \mathbf{S}^2 \rangle$ values and ZP+thermal (T = 298 K) energies, as well as some geometric parameters

TABLE 2: Relative Energies of the Stationary States in the X−H + Y• → X• + H−Y Reaction[a]

X	Y	struct	UMP2	PMP2//UMP2	CCSD(T)//UMP2	DFT (B3LYP)	expt
CH_3	CH_3	R	0	0	0	0	0
(Figure 1)[b]		RC′	(−0.3)	(−0.3)	(−0.3)		
		RC(**1**)	(−0.4)	(−0.4)	(−0.4)		
		TS(**1**)	18.6	16.4	17.6	14.6	14 to 14.5[g]
					17.7[c]		
CH_3	NH_2	R	0	0	0	0	0
(Figure 2)[b]		RC(**2**)	(−0.9)	(−0.9)	(−0.9)	(−0.4)	
		TS(**2**)	14.8	12.3	14.9	10.8	∼10.5[i]
					15.0[d]		
		PC(**2**)	(−5.3)	(−5.3)	(−2.5)	(−3.0)	
		PC′(**2**)	(−4.8)	(−4.8)	(−1.9)	(−2.5)	
		P	−3.9	−3.8	−0.9	−1.6	−2.6 to −3.4[h]
CH_3	OH	R	0	0	0	0	0
(Figure 3)[b]		RC′				(−0.3)	
		RC(**3**)	(−0.9)	(−0.8)	(−0.9)	(−0.5)	
		TS(**3**)	8.0	5.9	6.7	0.6	3−6[j]
					6.8[d]		
		PC(**3**)	(−16.0)	(−16.0)	(−11.4)	(−12.4)	
		P	−15.7	−15.7	−11.1	−11.9	−14.5 to −14.8[h]
NH_2	NH_2	R	0	0	0	0	0
(Figure 4)[b]		RC′(**4**)	(−3.9)	(−3.9)	(−3.8)	(−3.6)	
		RC(**4**)	(−2.9)	(−2.9)	(−2.8)	(−2.4)	
		TS(**4**)	12.7	9.6	12.0	5.6	9.5 to 15[k]
					11.9[c]		
NH_2	OH	R	0	0	0	0	0
(Figure 5)[b]		RC(**5**)				(−5.2)	
		RC′(**5**)	(−8.0)	(−8.0)	(−7.8)	(−8.3)	
		TS(**5**)	7.5[n]	5.3	4.1	−4.2[o]	2.6[l]
					4.2[d]		
		PC(**5**)	(−16.1)[n]	(−16.2)	(−14.2)	(−14.3)[o]	
		P	−11.8	−11.9	−10.2	−10.3	−11.4 to −11.9[h]
OH	OH	R	0	0	0	0	0
(Figure 6)[b]		RC(**6**)	(−3.7)	(−3.7)	(−3.7)		
		RC′(**6**)	(−6.4)	(−6.4)	(−6.3)	(−6.3)	
		TS(**6**)[e]	10.9	8.1	8.7		5.3[m]
		SS(**6**)[f]	(11.7)	(7.9)	(10.3)	(1.3)	5.3[m]
					(9.9)[c]		

[a] Energies in kcal/mol; corrected for ZP+thermal (T = 298 K) energy differences, except for the RC, PC, and SS energies (in parentheses), which are uncorrected. [b] Figure numbers in parentheses. [c] One-dimensional symmetric X···H distance CCSD(T) optimization. [d] One-dimensional optimization using the UMP2 IRC geometries about the TS. [e] Asymmetric TS. [f] Symmetric structure; TS(DFT) or minimum(UMP2). [g] E_a from ref 52. [h] From refs 53 and 54. [i] E_a from ref 58. [j] E_a from refs 60−61, 64−67, and 69. [k] Estimate of E_a; see text. [l] E_a from ref 76. [m] E_a from ref 77. [n] Structure a in Figure 5. [o] Structure b in Figure 5.

for the UMP2 optimized structures at each stage (eq 1) of the reactions. Table 4 lists the corresponding data for the DFT(B3LYP) calculations. Both tables also contain the values of the imaginary frequency at each TS geometry. A summary of the internal angles in all the structures shown in the figures is presented in Table 5. The atomic spin density populations at the UMP2 and DFT(B3LYP) levels are found in Tables 6 and 7, respectively. The UMP2 populations were generated using the energy derivative method.[48] Figures **1**−**6** display the RC, TS, and PC type structures for all six reactions.

(1) $CH_4 + CH_3^• \rightarrow CH_3^• + CH_4$. Reaction 1 has been studied theoretically by various groups.[23−26,40,49−51] The CH_4···CH_3 reaction complex shown in Figure 1 [RC(**1**)] is very weakly bound, if at all. The UMP2 calculated C···C distance in RC(**1**) is 3.874 Å (Table 3). The PMP2 and CCSD(T) theory levels based on the UMP2 geometry optimization both give a purely electronic energy for RC(**1**) of only −0.4 kcal/mol relative to reactants, not counting BSSE. In these discussions reaction and product complex energies lower than the reactants will carry a minus sign and the corresponding binding energies will be positive. DFT(B3LYP) gives no energy minimum at all, and a stable reaction complex structure was not found. The UMP2 level RC(**1**) geometry is not on the least motion path for reaction (1) and doesn't have the CH_3−H···CH_3 hydrogen-bonding form, but looks rather more like a van der Waals complex. The failure of DFT(B3LYP) to give such an electronically bound structure for such a complex is, therefore, not surprising.[47] If this complex is not electronically stable, then the UMP2 binding energy is due to BSSE. The UMP2 atomic spin density population distribution in RC(**1**) looks almost exactly like the reactants with the unpaired spin localized mainly in the methyl σ orbital perpendicular to the C···C axis.

A UMP2 optimized geometry that does look like a reaction complex on the CH_3−H···CH_3 hydrogen atom transfer path was found (RC′) with a H···C distance of 3.185 Å. However, RC′ has two small imaginary frequencies in the harmonic force field analysis and a slightly smaller (∼0.1 kcal/mol) total energy relative to RC(**1**). The imaginary frequencies indicate that this higher energy RC′ structure is a rotamer transition state leading to RC(**1**). Since the ZP+thermal (T = 298 K) energies for RC(**1**) are 1.8 kcal/mol larger than for the reactants (Table 3), the purely electronic binding energy of 0.4 kcal/mol is overwhelmed and RC(**1**) will spontaneously dissociate back to reactants.

The failure in this study to find a stable CH_3−H···CH_3 reaction complex at the DFT(B3LYP) electronic structure level is similar to that reported by others using both the GGA[24] and DFT hybrid functional[26a] methods. Most of the theory levels applied[24,26a,50] find, as here for UMP2 (Table 1), an electronic binding energy for this complex relative to reactants of only ∼0.4 kcal/mol, but vary considerably in the H···C distance between 2.5 and 3.4 Å. The extensive DFT hybrid functional calculations of Jursic[26a] show increasing values of the H···C distance with increasing basis set size, as the pure electronic

TABLE 3: Calculated UMP2 Properties of the Stationary States in the X−H′ + Y• → X• + H′−Y Reaction[a]

X AH_n	Y BH_m	struct	$\langle S^2 \rangle$	iω[c] (cm^{-1})	ZP+ thermal[d]	A−H′ (Å)	H′−B (Å)	A−H′−B (deg)	A···B (Å)
CH_3	CH_3	R	0.7615		51.3	1.089			
(Figure 1)[b]		RC′	0.7616	v. sm	51.8	1.089	3.185	175.6	4.271
		RC(**1**)[g]	0.7615		53.1				3.874
		TS(**1**)	0.7877	1960	50.2	1.327	1.327	180.0	2.654
						1.342[m]	1.342[m]		
CH_3	NH_2	R	0.7593		44.3	1.089			
(Figure 2)[b]		RC(**2**)	0.7593		46.2	1.089	2.797	179.8	3.886
		TS(**2**)	0.7903	2074	43.4	1.277	1.283	169.1	2.549
						1.302[n]	1.259[n]		
		PC(**2**)[h]	0.7613		46.3	1.079	2.656	179.9	3.736
		PC(**2**)	0.7615		46.3	2.791	1.015	165.0	3.781
		P	0.7615		44.4		1.014		
CH_3	OH	R	0.7566		37.3	1.089			
(Figure 3)[b]		RC′							
		RC(**3**)[i]	0.7565		38.7	2.650	0.973	154.1	3.550
		TS(**3**)	0.7804	1846	35.4	1.192	1.322	168.8	2.502
						1.219[n]	1.294[n]		
		PC(**3**)	0.7613		38.0	2.480	0.966	162.9	3.414
		P	0.7615		36.1		0.963		
NH_2	NH_2	R	0.7593		37.4	1.014			
(Figure 4)[b]		RC′(**4**)[j]	0.7592		39.5	2.285	1.029	166.0	3.293
		RC(**4**)	0.7593		39.5	1.017	2.331	158.2	3.297
		TS(**4**)	0.7979	269	36.9	1.230	1.230	153.6	2.395
						1.247[m]	1.247[m]		
NH_2	OH	R	0.7566		30.4	1.016			
(Figure 5)[b]		RC(**5**)							
		RC′(**5**)[k]	0.7564		32.8	1.942	0.987	179.8	2.929
		TSa(**5a**)	0.7809	2397	29.0	1.110	1.312	148.3	2.331
						1.134[m]	1.289[m]		
		PCa(**5a**)	0.7594		31.4	2.042	0.971	173.3	3.009
		P	0.7593		29.1		0.963		
OH	OH	R	0.7566		22.1	0.963			
(Figure 6)[b]		RC(**6**)	0.7566		23.8	0.967	2.100	152.5	2.991
		RC′(**6**)[l]	0.7564		24.1	1.927	0.979	178.3	2.905
		TS(**6**)[e]	0.7868	2475	21.0	1.110	1.199	141.9	2.183
		SS(**6**)[f]	0.7974		25.5	1.146	1.146	140.7	2.158
						1.164[n]	1.164[n]		

[a] RC = X−H′···Y, TS = X···H′···Y, and PC = X···H′−Y, unless otherwise noted. X = AH_n and Y = AH_m.. [b] Figure numbers in parentheses. [c] Imaginary frequency from harmonic force field analysis for TS. [d] Zero point vibrational+thermal (T = 298 K) energy; see text. [e] Asymmetric TS. [f] Symmetric structure; TS(DFT) or minimum(UMP2). [g] CH_4···CH_3; H′ is not defined. [h] X−H′···Y = CH_2−H′···NH_3. [i] X···H′−Y = CH_4···H′−O. [j] X···H′−Y = NH_3···H′−NH. [k] X···H′−Y = NH_3···H′−O. [l] X···H′−Y = H_2O···H′−O. [m] One-dimensional symmetric X···H distance CCSD(T) optimization. [n] One-dimensional optimization using the UMP2 IRC geometries about the TS.

binding energy decreases to 0.01 kcal/mol for the largest basis set. Therefore, the least motion path CH_3−H···CH_3 hydrogen-bonded complex apparently does not exist within GGA or hybrid DFT theory and may not be sufficiently bound to be a factor in interpreting experimental kinetic data.

The calculated CH_3···H···CH_3 TS(**1**) structure looks the same at both the UMP2 and DFT(B3LYP) levels. The geometry is symmetric, with a linear C···H···C connectivity and perfectly staggered methyl groups with equivalent hydrogen atoms. The equilibrium C···H distances are 1.327 Å (UMP2) and 1.346 Å (DFT) from Tables 3 and 4, respectively, which are very close. The ZP+thermal (T = 298 K) energy for the reactants is 1.1 (UMP2) or 1.0 (DFT) kcal/mol larger than for TS(**2**). This correction must, therefore, be subtracted from the total electronic energy differences (the barrier height) to give activation energies of 18.6 (UMP2), 16.4 (PMP2), 17.6 [CCSD(T)], and 14.6 (DFT) kcal/mol.

The experimental activation energy (E_a), obtained by fitting temperature dependent kinetic data to the Arrehenius functional form, is 14.0−14.5 kcal/mol at room temperature.[52] This latter quantity represents a statistical average of reaction paths over the potential energy surface. The Arrehenius fit neglects temperature effects in the prefactor of the Arrehenius functional form and doesn't explicitly account for quantum mechanical tunneling through the barrier. The net result of these simplifications is a certain uncertainty in relating the calculated R → TS activation energy to the Arrehenius fitted activation energy, although the neglect of tunneling should give an effectively smaller fitted Arrehenius E_a compared to the calculated reaction path value.[49c] In this study for the CH_4 + CH_3• → CH_3• + CH_4 hydrogen exchange reaction, DFT(B3LYP) predicts the lowest activation barrier and gives good numerical agreement with the Arrehenius E_a. A symmetric one-dimensional CCSD(T) pointwise optimization of the C···H distances in TS(**1**) increases their value to 1.342 Å, which is almost the same as the 1.346 Å DFT(B3LYP) length, and lowers the CCSD(T) barrier by 0.1 kcal/mol to an adjusted 17.5 kcal/mol (Table 2). Therefore, the next best numerical agreement with experiment is the 16.4 kcal/mol calculated for E_a by the PMP2 method. Since, as noted above, the theoretical activation energy at the transition state is expected to be somewhat larger than the Arrehenius fitted experimental value, the PMP2 and CCSD(T) barrier energies are probably somewhat closer to the expected theoretical value than DFT.

The calculated UHF and DFT $\langle S^2 \rangle$ values for R, RC(**1**), and TS(**1**) structures, shown in Tables 3 and 4, are close to the exact 0.75 value for S = 1/2. The DFT $\langle S^2 \rangle$ are consistently smaller than the corresponding UHF structure values. The largest calculated $\langle S^2 \rangle$ value is for the UMP2 TS, and it is reduced to 0.7506 after annihilation of the first spin contaminant (S = 3/2).

TABLE 4: Calculated DFT(B3LYP) Properties of the Stationary States in the X−H′ + Y• → X• + H′−Y Reaction[a]

X AH_n	Y BH_m	struct	$\langle S^2 \rangle$	iω[c] (cm^{-1})	ZP+ thermal[d]	A−H (Å)	H′−B (Å)	A−H′−B (Å)	A···B (Å)
CH_3	CH_3	R	0.7535		50.3	1.090			
(Figure 1)[b]		TS(**1**)	0.7570	1642	49.2	1.346	1.346	180.0	2.692
CH_3	NH_2	R	0.7532		43.4	1.090			
(Figure 2)[b]		RC(**2**)	0.7531	23	44.7	1.090	2.851	179.6	3.941
		TS(**2**)	0.7576	1662	42.6	1.322	1.276	171.2	2.590
		PC(**2**)[g]	0.7535	24	45.1	1.082	2.653	179.8	3.735
		PC′(**2**)	0.7535		45.6	2.742	1.017	170.9	3.750
		P	0.7535		43.8		1.015		
CH_3	OH	R	0.7525		36.5	1.090			
(Figure 3)[b]		RC′	0.7526		38.0	1.093	2.956	143.3	3.239
		RC(**3**)[h]	0.7524		38.0	2.655	0.978	176.8	3.631
		TS(**3**)	0.7569	906	34.7	1.216	1.322	172.8	2.534
		PC(**3**)	0.7535		36.9	2.386	0.968	179.0	3.353
		P	0.7535		35.6		0.963		
NH_2	NH_2	R	0.7532		37.0	1.015			
(Figure 4)[b]		RC′(**4**)[i]	0.7531		39.0	2.258	1.034	170.2	3.282
		RC(**4**)	0.7532		39.0	1.018	2.336	165.6	3.332
		TS(**4**)	0.7588	1,614	36.2	1.250	1.250	157.6	2.452
NH_2	OH	R	0.7525		30.1	1.015			
(Figure 5)[b]		RC(**5**)	0.7558		31.9	1.013	2.189	93.6	2.469
		RC′(**5**)[j]	0.7525		32.2	1.906	0.995	179.9	2.902
		TSb(**5b**)	0.7584	1,194	28.6	1.155	1.272	151.1	2.351
		PCb(**5b**)	0.7532		31.1	2.007	0.973	171.2	2.972
		P	0.7532		28.8		0.963		
OH	OH	R	0.7525		21.9	0.963			
(Figure 6)[b]		RC(**6**)							
		RC′(**6**)[k]	0.7524		23.9	1.891	0.985	176.8	2.875
		TS(**6**)[e]							
		SS(**6**)[f]	0.7578	1474	20.6	1.166	1.166	145.7	2.228

[a] RC = X−H′···Y, TS = X···H′···Y, and PC = X···H′−Y, unless otherwise noted; X = AH_n and Y = AH_m. [b] Figure numbers in parentheses. [c] Imaginary frequency from harmonic force field analysis for TS. [d] Zero-point vibrational+thermal (T = 298 K) energy; see text. [e] Asymmetric geometry. [f] Symmetric structure; TS(DFT) or minimum (UMP2). [g] X−H′···Y = CH_2−H′···NH_3. [h] X···H′−Y = CH_4···H′−O. [i] X···H′−Y = NH_3···H′−NH. [j] X···H′−Y = NH_3···H′−O. [k] X···H′−Y = H_2O···H′−O.

TABLE 5: Bond Angles in the Stationary States of the X−H′ + Y• → X• + H′−Y Reactions[a]

				UMP2			DFT(B3LYP)	
X	Y	struct	H_a	H_a−A−H′	H′−B−H_b	H_b	H_a−A−H′	H′−B−H_b
CH_3	CH_3	TS(**1**)	H	105.3	105.3	H	105.1	105.1
(Figure 1)[b]								
CH_3	NH_2	RC(**2**)	H	109.7	128.2	H	109.7	128.3
(Figure 2)[b]		TS(**2**)	H_3, H_4	104.4	100.2	H	103.5	101.0
			H_5	108.7		H_1, H_2	108.3	
CH_3	OH	TS(**3**)	H_5	108.4	98.0	H_2	107.7	99.6
(Figure 3)[b]			H_6, H_7	105.7			104.7	
		PC(**3**)	H_3	103.9	104.0[n]	H_2	99.6	105.1
			H_4	94.5			92.5	
			H_5	78.9			85.1	
NH_2	NH_2	RC′(**4**)[e]	H_3, H_4	118.2	104.0	H_2	116.5	103.7
(Figure 4)[b]			H_5	98.5			101.9	
		RC(**4**)	H_4, H_5	107.2	151.4	H_2	107.4	146.6
					101.8	H_3		109.4
		TS(**4**)	H_4, H_5	107.2	107.2	H_2, H_3	107.5	107.5
NH_2	OH	RC′(**5**)[f]	H_2	112.1		H_2	111.8	
(Figure 5)[b]		H_3, H_4	111.8			H_3, H_4	111.6	
		TS(**5**)	H_3	107.5	107.6	H_2	110.7	107.5
			H_4	107.0			108.5	
		PC(**5**)	H_3	127.0	104.8	H_2	137.7	105.5
			H_4	127.0				117.6
OH	OH	RC(**6**)	H_3	105.2	100.3	H_2		
(Figure 6)[b]		RC′(**6**)[g]	H_2, H_3	121.6			119.5	
		TS(**6**)[c]	H_3	103.1	103.5	H_2		
		SS(**6**)[d]	H_3	104.7	104.7	H_2	105.2	105.2

[a] Angles in degrees. A is the heavy atom in X and B is the heavy atom in Y. H′ is being abstracted. RC = X−H′···Y, TS = X···H′···Y, and PC = X···H′−Y, unless otherwise indicated. [b] Figure numbers in parentheses. [c] Asymmetric TS. [d] Symmetric structure; TS(DFT) or minimum(UMP2). [e] X···H′−Y = NH_3···H′−NH. [f] X···H′−Y = NH_3···H′−O. [g] X···H′−Y = H_2O···H′−O.

This illustrates why PMP2 predicts a better barrier height than UMP2.

Both the UMP2 and DFT spin densities for TS(**1**) show the electron spin to be concentrated on the carbon atoms and symmetrically distributed along the C···H···C axis (Tables 6 and 7). In a single-configuration RHF wave function for this transition state the unpaired electron would be in an orbital that has a node at the bridging hydrogen atom, whose spin population would then be zero. The small negative spin population calculated here reflects both spin polarization and spin con-

TABLE 6: Atomic Spin Populations from the UMP2 α and β Spin Density Matrices[a]

AH_n	BH_m	struct	H(A)		A	H′	B	H(B)	
CH_3	CH_3	R		0	0	0	1.207		0.069
(Figure 1)[b]		TS(**1**)	(H)	−0.018	0.622	−0.133	0.622	(H)	−0.018
CH_3	NH_2	R		0	0	0	1.099		−0.050
(Figure 2)[b]		RC(**2**)	(H)	0	0	0.002	1.099	(H)	−0.049
		TS(**2**)	(H_3, H_4)	−0.013	0.516	−0.049	0.601	(H_2, H_2)	−0.012
			(H_5)	−0.019					
		P		−0.069	1.207	0	0		0
CH_3	OH	R		0	0	0	1.033		−0.033
(Figure 3)[b]		TS(**3**)	(H_3)	−0.015	0.399	−0.049	0.702	(H_2)	−0.017
			(H_4)	−0.010					
			(H_5)	−0.009					
		PC(**3**)	(H_3, H_4, H_5)	−0.064	1.184	0.005	0.002	(H_2)	−0.001
			(H_3)	−0.063					
		P		−0.069	1.207	0.002	0		0
NH_2	NH_2	R		0	0	0	1.099		−0.050
(Figure 4)[b]		RC′(**4**)[c]	(H_3, H_4, H_5)	0	0	−0.056	1.105	(H_2)	−0.050
		RC(**4**)	(H_4, H_5)	0	0.001	−0.002	1.100	(H_2, H_3)	−0.049
		TS(**4**)	(H_4, H_5)	−0.012	0.521	0.008	0.521	(H_2, H_3)	−0.012
NH_2	OH	R		0	0	0	1.033		−0.033
(Figure 5)[b]		RC′(**5**)[d]	(H_3, H_4, H_5)	0	0	−0.032	1.033		
		TS(**5a**)	(H_3, H_4)	−0.013	0.393	−0.012	0.666	(H_2)	−0.021
		PC(**5a**)	(H_3, H_4)	−0.049	1.104	−0.008	0.002	(H_2)	0
		P		−0.050	1.099	0	0		0
OH	OH	R		0	0	0	1.033		−0.033
(Figure 6)[b]		RC(**6**)	(H_3)	−0.001	0	−0.03	1.040	(H_2)	−0.036
		RC′(**6**)[e]	(H_2, H_3)	0	0	−0.034	1.034		
		TS(**6**)[f]	(H_3)	−0.013	0.422	−0.013	0.620	(H_2)	−0.017
		SS(**6**)[g]	(H_3)	−0.013	0.504	0.019	0.504	(H_2)	0.013

[a] Structures represented as RC = AH_n−H′···BH_m, TS = AH_n···H′···BH_m, and PC = AH_n···H′−BH_m, unless otherwise noted. [b] Figure numbers in parentheses. [c] NH_3···H′−NH. [d] NH_3···H′−O. [e] H_2O···H′−O. [f] Assymetric geometry; saddle point. [g] Symmetric geometry; energy minimum.

TABLE 7: Atomic Spin Populations from the DFT(B3LYP) α and β Spin Density Matrices[a]

AH_n	BH_m	struct	H(A)		A	H′	B	H(B)	
CH_3	CH_3	R		0	0	0	1.161		−0.054
(Figure 1)[b]		TS(**1**)	(H)	−0.016	0.598	−0.101	0.518	(H)	−0.016
CH_3	NH_2	R		0	0	0	1.077		−0.039
(Figure 2)[b]		RC(**2**)	(H)	0	0	0.001	1.077	(H)	−0.039
		TS(**2**)	(H_3, H_4)	−0.013	0.554	−0.028	0.554	(H_1, H_2)	−0.010
			(H_5)	−0.018					
		P		−0.054	1.161	0	0		0
CH_3	OH	TS(**3**)	(H_3)	−0.012	0.426	−0.019	0.635	(H_2)	−0.015
(Figure 3)[b]			(H_4)	−0.008					
			(H_5)	−0.007					
		PC(**3**)	(H_3, H_4, H_5)	−0.049	1.131	0.001	0.012	(H_2)	0.004
		P		−0.053	1.158	0	0		0
NH_2	NH_2		R	0	0	0	1.077		0.038
(Figure 4)[b]		RC′(**4**)[c]	(H_3, H_4, H_5)	0	0.001	−0.041	1.079	(H_2)	−0.039
		RC(**4**)	(H_4, H_5)	0	0.001	−0.003	1.079	(H_2, H_3)	−0.038
		TS(**4**)	(H_4, H_5)	−0.013	0.535	−0.018	0.535	(H_2, H_3)	−0.013
NH_2	OH	R		0	0	0	1.027		−0.027
(Figure 5)[b]		RC(**5**)	(H)	−0.005	0.227	−0.005	0.808		−0.020
		RC′(**5**)[d]	(H_2, H_3, H_4)	0	0	−0.026	1.026		
		TS(**5b**)	(H_3, H_4)	−0.016	0.555	−0.016	0.507	(H_2)	−0.014
		PC(**5b**)	(H_3, H_4)	−0.038	1.079	−0.006	0.005	(H_2)	−0.001
		P		−0.039	1.077	0	0		0
OH	OH	R		0	0	0	1.027		−0.027
(Figure 6)[b]		RC′(**6**)[e]	(H_2, H_3)	0.001	0	−0.026	1.025		
		SS(**6**)[f]	(H_3)	−0.014	0.525	−0.022	0.525	(H_2)	−0.014

[a] Structures represented as RC = AH_n−H′···BH_m, TS = AH_n···H′···BH_m, and PC = AH_n···H′−BH_m, unless otherwise noted. [b] Figure numbers in parentheses. [c] NH_3···H′−NH. [d] NH_3···H′−O. [e] H_2O···H′−O. [f] Symmetric geometry; TS.

tamination. The magnitude of the latter effect can be gauged from the generally smaller negative spin populations in the DFT method (Table 7) compared to UMP2 (Table 6).

The location and energy barrier of TS(**1**) calculated here agrees well with previous work, both at the MP2[40,49−51] and DFT levels.[23−26] MP4 energy calculations[50,51] at optimized MP2 geometries reduce the calculated barrier height somewhat relative to MP2, as found here also for the CCSD(T) level of theory. The imaginary frequency at the TS, corresponding to an antisymmetric motion of the bridging hydrogen atom along the C···H···C axis, is calculated here to be 1960 (MP2, Table 2) and 1642 (DFT, Table 3) cm^{-1}. Previous predicted values,[49−51] all at post-Hartree−Fock levels, are in the 2000−2500 cm^{-1} range, decreasing as the theory level improves. The same trend is found for the barrier height energy. These two quantities, representing the curvature (or width) and height of the barrier, respectively, are important for the modeling of the kinetic data, including tunneling effects.[37a,49−51]

(2) $CH_4 + NH_2^\bullet \rightarrow CH_3^\bullet + NH_3$. For reaction 2, the most stable CH_3···NH_3 product complex, PC(**2**), obtained at both the

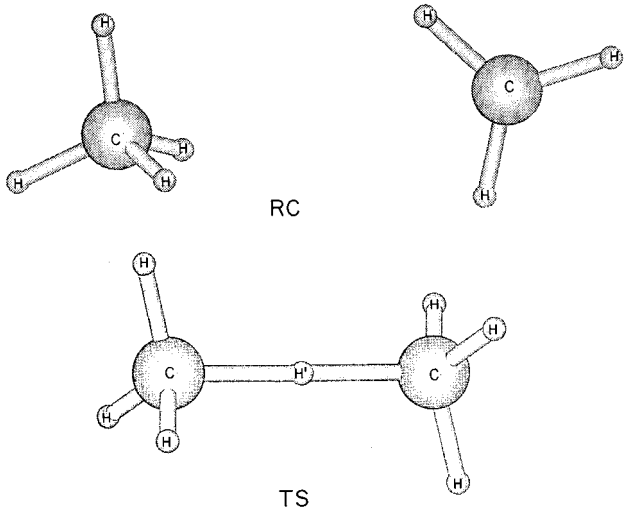

Figure 1. Geometries of RC and TS for the $CH_4 + CH_3^{\bullet}$ reaction.

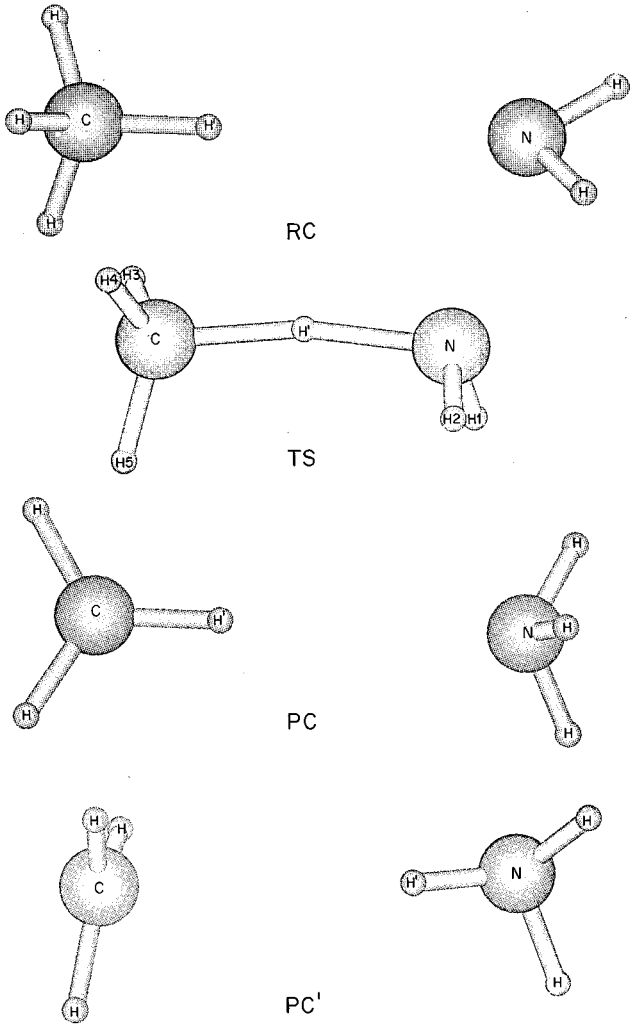

Figure 2. Geometries of RC, TS, PC, and PC′ for the $CH_4 + NH_2^{\bullet}$ reaction.

UMP2 and DFT(B3LYP) levels, actually has a $CH_2-H\cdots NH_3$ structure and does not lie on the least motion reaction path. Ammonia is clearly more nucleophilic than CH_3. A $CH_3\cdots H-NH_2$ complex [PC′(**2**)] was also found at both the UMP2 and DFT(B3LYP) levels with an electronic energy 0.5 kcal/mol above PC(**2**) in both methods (Table 2), having a N···H−C angle of 165.0° (UMP2) or 170.9° (DFT) and a C···H distance of 2.791 Å (UMP2) or 2.742 Å (DFT), shown in Tables 3 and

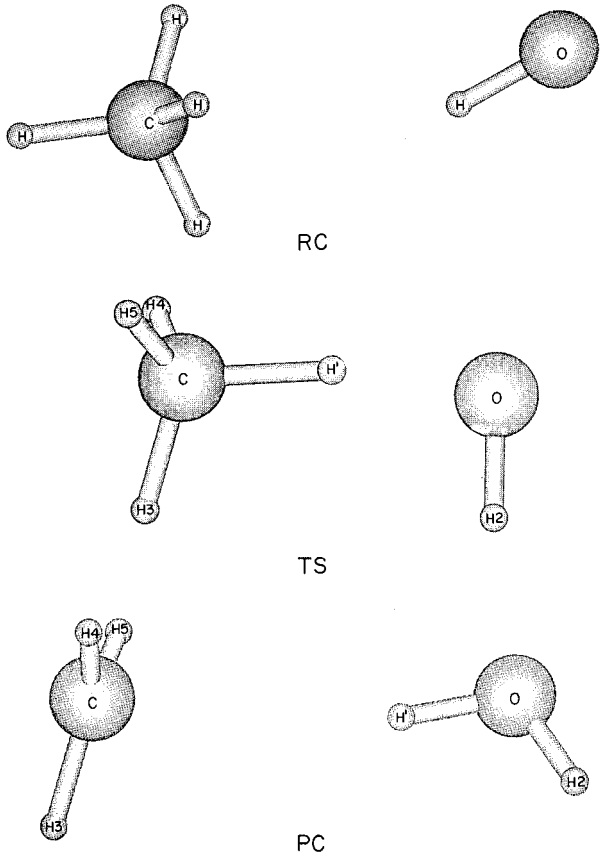

Figure 3. Geometries of RC, TS, and PC for the $CH_4 + OH^{\bullet}$ reaction.

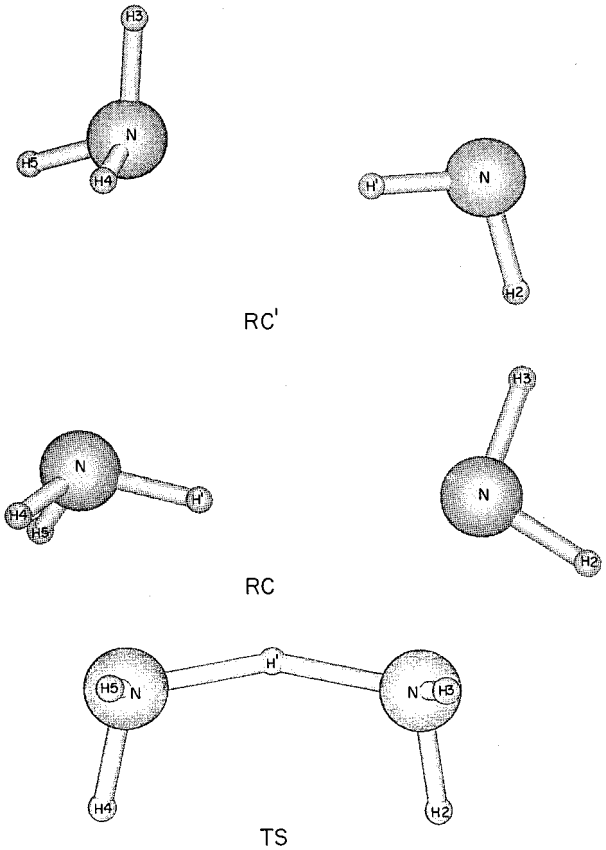

Figure 4. Geometries of RC′, RC, and TS for the $NH_3 + NH_2^{\bullet}$ reaction.

4. This weak complex shows all real harmonic force field frequencies characteristic of a minimum energy structure. The unpaired spin density distribution in PC(**2**), PC′(**2**) and P are similar (Tables 6 and 7) except for the spatial orientation of

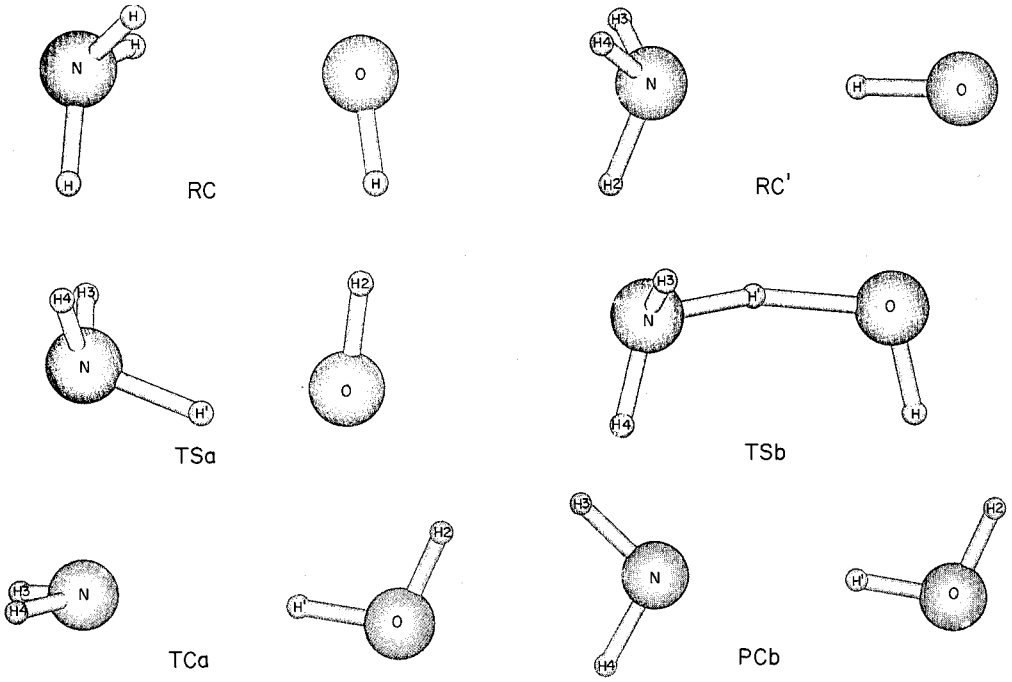

Figure 5. Geometries of RC, RC′, TSa, TSb, PCa, and PCb for the $NH_3 + OH^\bullet$ reaction.

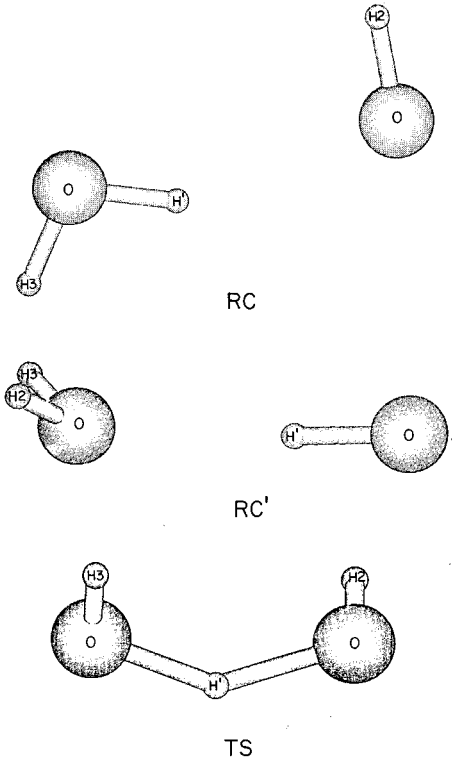

Figure 6. Geometries of RC, RC′, and TS for the $H_2O + OH^\bullet$ reaction. SS is similar to TS.

the radical electron relative to the geometric structure. In this aspect, the >C−H···N part of PC(**2**) is planar and the unpaired spin is directed mainly perpendicular to this plane, while PC′(**2**) has its unpaired spin concentrated along the C···H−N< axis. In both cases the spin is located in the methyl group σ orbital. The MP2 and DFT geometries for PC(**2**) have the same relative orientation of the NH_3 and CH_2 hydrogen atoms. The H···N distance is also similar in both structures, 2.656 Å (MP2) and 2.653 Å (DFT).

The MP2, PMP2, and DFT(B3LYP) electronic energies for PC(**2**) are 1.4 kcal/mol more stable than the combined reactants, and this stability is only 1.0 kcal/mol at the CCSD(T) level (Table 2). Since the ZP+thermal (T = 298 K) energy differences between P and PC(**2**) shown in Tables 3 and 4 are, respectively, 1.9 (MP2) and 1.3 (DFT) kcal/mol larger in PC(**2**), the electronic binding energy is canceled and the reaction complex is unbound. The ZPE only difference is 1.1 (UMP2) or 1.0 (DFT) kcal/mol so that at very low temperature the shallow energy minimum may be able to support PC(**2**) at the zero-point vibrational energy level. The binding situation with regard to PC′(**2**) is less favorable.

Experimentally, the thermodynamics of the $CH_4 + NH_2^\bullet \rightarrow CH_3^\bullet + NH_3$ reaction favor the products by 2.6[53] to 3.4[54] kcal/mol. A straightforward application of G2 theory[41,55] to the reactant and product species gives a calculated exothermicity of 2.1 kcal/mol for this reaction. Therefore, by the Hammond principle[56] the geometric structure of the transition state TS(**2**) is expected to be somewhat closer to CH_3−H···NH_2 than to CH_3···H−NH_2. The calculated C···H and H···N distances in TS(**2**) are 1.277 and 1.283 Å, respectively, at the UMP2 level, compared to C−H and H−N bond lengths in isolated CH_4 and NH_3, respectively, of 1.089 and 1.014 Å (Table 3). Therefore, as anticipated, the UMP2 level TS(**2**) structure is relatively closer to the reactants. At the DFT(B3LYP) theory level the calculated reaction energy of −1.6 kcal/mol, after a differential 0.4 kcal/mol ZP+thermal (T = 298 K) correction from Table 4, is smaller than for UMP2 (−3.9 kcal/mol after a 0.1 kcal/mol correction from Table 3). The DFT(B3LYP) TS(**2**) structure C···H and H···N bond lengths are 1.322 and 1.276 Å, respectively, closer to CH_3···H−NH_2 and to the bond length difference in the isolated molecules. The calculated interaction distance relationships between C···H and H···N for TS(**2**) also dictate the unpaired spin density distributions (Tables 6 and 7). The radical electron is heavily concentrated on the N atom at the UMP2 level, where the C···H distance is shorter, but shows more equal densities on the C and N atom at the DFT level, where C···H is longer. In both cases the radical electron is localized along the mildly bent C···H···N axis. The DFT interaction bond lengths are less consistent with the Hammond principle.[56] The geometric configuration in both methods has the remote C−H and N−H bond in a staggered conformation. Therefore, the major difference between the UMP2 and DFT

structures for TS(**2**) is in the C···H distance, which is 0.045 Å longer in DFT.

The activation energy for the $CH_4 + NH_2^\bullet \rightarrow CH_3^\bullet + NH_3$ reaction, as obtained by fitting experimental kinetic data to Arrehenius plots in different temperature ranges, has been reported as 15.2 kcal/mol (2100 K ≥ T ≥ 1500 K),[57a] 13.2 kcal/mol (1023 K ≥ T ≥ 743 K),[57b] 11.2 kcal/mol (T = 600 K),[58] and 10.3 kcal/mol (520 K > T 300 K).[59] The temperature dependence of the Arrehenius activation energy is, among other factors, an indication of a tunneling effect in the kinetics of the reaction. The recommended value of E_a for the above reaction for comparison to theory is ∼10.5 kcal/mol.[59] As noted above, because of the tunneling effect, the *ab initio* calculated activation energy should be somewhat larger than the Arrehenius fitted value. After adjustment for ZP+thermal (T = 298 K) energy differences between reactants and TS(**2**), the UMP2 and CCSD(T) calculated activation energies (Table 2) are 14.8 and 14.9 kcal/mol, respectively, while PMP2 and DFT(B3LYP) give 12.3 and 10.3 kcal/mol, respectively. Again, as with the $CH_4 + CH_3^\bullet \rightarrow CH_3^\bullet + CH_4$ reaction, the PMP2 calculated value comes closest to experiment from above. The DFT calculated barrier agrees nicely with the recommended activation barrier, but is lower than the expected theoretical TS energy, which should be somewhat larger than 10.5 kcal/mol.

CCSD(T) energies were also calculated at IRC points on both sides of the UMP2 optimized transition state and the maximum energy interpolated in a quasi-one-dimensional optimization of the TS at this theory level.[44] The calculated extremum CCSD(T) energy increases by only 0.1 kcal/mol relative to reactants (Table 2), but the C···H (1.302 Å) and H···N (1.259 Å) distances in the new geometric structure are closer to the DFT TS(**4**) geometric structure (Table 3). This result is consistent with the lower CCSD(T) reaction exothermicity. Previous *ab initio* calculations at a lower theory level gave a −1.3 kcal/mol enthalpy of reaction in the forward direction and a TS structure with a C···H distance of 1.261 Å and a H···N distance of 1.341 Å, consistent with the present UMP2 results[40] at least in the relative bond lengths.

RC(**3**) has a CH_3−H···NH_2 structure that is in the entrance channel of the least motion reaction path for both UMP2 and DFT(B3LYP). The UMP2, PMP2, CCSD(T), and DFT binding energies of RC(**2**) relative to reactants are 0.9, 0.8, 0.8, and 0.4 kcal/mol, respectively. Since the ZP+thermal (T = 298 K) energy differences between RC(**3**) and R are 1.9 (UMP2) and 1.3 (DFT) kcal/mol, the reaction complex is also essentially unbound at room temperature at these theory levels. The ZPE energy differences alone are 0.8 (UMP2) or 0.7 (DFT) kcal/mol, which doesn't affect the above conclusion in a significant way.

The experimental ∼−3 kcal/mol reaction enthalpy[53,54] for the $CH_4 + NH_2^\bullet \rightarrow CH_3^\bullet + NH_3$ reaction (Table 2) is underestimated by DFT and even worse by CCSD(T) and overestimated at the UMP2 and PMP2 levels. The differences, however, are small, and the correct sign is obtained in all cases.

(3) $CH_4 + OH^\bullet \rightarrow CH_3^\bullet + H_2O$. Reaction 3 has been studied by *ab initio* methods,[26b,40,60−63,65] kinetic rate theory,[61,63−67] and experiment.[68,69] The most stable reaction complex, RC(**3**), does not have the expected CH_3−H···OH geometric structure and is not on the least motion reaction path. Instead, the CH_4···H−O interaction is preferred. The UMP2 and DFT optimized structures differ mainly in the C···H−O angle, which is 154.1° for UMP2 (Table 3) and 176.8° for DFT (Table 4). The calculated binding energies of RC(**3**) at the different theoretical levels are 0.8 to 0.9 kcal/mol [UMP2, PMP2, and CCSD(T)] and 0.5 kcal/mol (DFT). The DFT binding energy is smaller than the others and also has a somewhat larger C···O distance in the DFT geometry. However, the ZP+thermal (T = 298 K) energies of RC(**3**) are 1.4 (UMP2) and 1.5 (DFT) kcal/mol larger than for the combined reactants. These corrections are more than the calculated CH_4···H−O electronic binding energies at both the UMP2 and DFT levels, so that RC(**3**) is calculated to be unbound at room temperature. However, the ZPE differences alone are only 0.5 kcal/mol at both theory levels. Therefore, at very low temperature this complex may exist. The unpaired spin density in RC(**3**) is located mainly on the oxygen atom in the direction perpendicular to the C···H−O axis. The exact values of the spin populations are tabulated in Tables 6 and 7.

A CH_3−H···OH reactant complex (RC′) with C_s symmetry was found only at the DFT(B3LYP) level with an electronic binding energy of 0.3 kcal/mol relative to reactants. For this structure the H···O distance is 2.296 Å and the C−H···O angle is 143.3°. The hydroxyl hydrogen atom makes a 93.6° angle with the (C−)H···O direction. Given the differential ZP+thermal energy correction, this conformer is certainly unbound relative to reactants. In RC′ the radical electron on the oxygen atom is in the σ C−H···O bond axis. Starting with the DFT optimized PC′ geometry, UMP2 gradient optimization spontaneously and with no barrier gave the RC(**3**) structure.

The activation energy for the forward $CH_4 + OH^\bullet$ reaction is difficult to determine experimentally from temperature dependent kinetic studies because of the curvature in the Arrehenius plots.[64,69] This issue has been treated by a variety of combined experimental and theoretical techniques, including quantum tunneling effects.[60,61,64−67,69] The accepted E_a value for the forward reaction ranges from 3 to 6 kcal/mol,[60,61,63,64,69] with recommended values of 4.5[64] and 5.2[70] kcal/mol. The calculated UMP2, PMP2, and CCSD(T) electronic transition state energies relative to reactants are 9.9, 7.8, and 8.6 kcal/mol, respectively (Table 2). The unscaled UMP2 ZP+thermal (T = 298 K) correction energy is 1.9 kcal/mol (Table 3), giving net activation energies of 8.0, 5.9, and 6.7 kcal/mol, respectively, at these theory levels. The only one of the methods that falls in the experimentally derived range quoted above is PMP2, and CCSD(T) at 6.7 kcal/mol falls just above that range. The DFT(B3LYP) calculated electronic barrier height is 2.4 kcal/mol, from which has to be subtracted 1.8 kcal/mol for the ZP+thermal (T = 298 K) energy difference, to give a net barrier height of 0.6 kcal/mol. This latter value is certainly too small. PMP2 and CCSD(T), therefore, seem to give the best results for the barrier activation energy of TS(**3**) in the $CH_4 + OH^\bullet$ hydrogen abstraction reaction. A previous high-level calculation for the saddle point energy in this reaction gave 7.4 kcal/mol,[63b] which, after correction for the ZP+thermal (T = 298 K) energy difference, gives an activation energy of 5.5 kcal/mol, close to the PMP2 value obtained here and to the recommended value.

The geometric structure of TS(**3**), CH_3···H···OH, shows the identical H···O distance of 1.322 Å using both the UMP2 and DFT methods. The C···H distance is shorter (1.192 Å) at the UMP2 theory level (Table 3) than at the DFT level (1.216 Å, Table 4). These bond lengths are consistent with the early transition state expected for an exothermic reaction.[56] Since, as will be discussed below, the DFT method predicts a smaller exothermicity for the forward reaction than UMP2, the C···H length in the TS is expected to be longer at the DFT theory level, as calculated. The H···O−H angle in TS(**3**) is almost perpendicular to the C···O axis (98.0° in UMP2 and 99.6° in DFT), and the O−H bond is essentially eclipsed[63b] with a methyl group C−H bond (H−C···O−H dihedral angle of 5.0° for both UMP2 and DFT). The near perpendicular orientation of O−H

relative to the C−H···O axis is also reflected in the spin density distribution that is localized along the hydrogen bond axis, which is the π direction for the hydroxyl group. The unpaired spin population on the oxygen atom is 0.702 (UMP2) or 0.635 (DFT), the smaller latter value reflecting the longer C···H distance at the DFT level. There is a factor of ∼2 difference between UMP2 and DFT in the calculated imaginary frequency at the TS that describes the incipient reaction paths in both the forward and reverse directions (Tables 3 and 4). This difference is consistent with the substantially lower calculated barrier height energy at the DFT level ($E_a = 0.6$ kcal/mol in Table 2) compared with UMP2. The calculated geometric structure and reaction path frequency (1846 cm^{-1}) calculated here by UMP2 agrees very well with previous highest level *ab initio* calculated properties for this TS.[61,63b] Finally, the one-dimensional IRC-(UMP2) optimization of TS(**3**) at the CCSD(T) level increases the saddle point energy relative to reactants by 0.1 kcal/mol (Table 2), lengthens C···H, and shortens the H···O bond lengths.

The product complex, PC(**3**), is on the least motion reaction path, with a CH_3···H−OH configuration in the exit channel. As expected from a hydrogen-bonded interaction with a methyl group, the calculated electronic binding energies relative to products (Table 2) are only from 0.3 to 0.5 kcal/mol. The ZPE difference alone between PC(**3**) and the $CH_3^\bullet + H_2O$ products is 1.1 kcal/mol (385 cm^{-1}) at both the UMP2 and DFT theory levels (Tables 3 and 4). The shallow adiabatic electronic energy minimum is, therefore, not able to bind the complex at the zero-point vibrational level. The 1.1 kcal/mol ZPE energy difference comes from converting six translational and rotational modes of the $CH_3^\bullet + H_2O$ species into vibrational modes of the complex. The absence of binding is probably not surprising given that the radical electron is localized on the methyl carbon atom (Tables 6 and 7) and oriented toward a water hydrogen atom. The methyl group is also tilted relative to the C···H−O axis (Table 5).

The exothermicity of the $CH_4 + OH^\bullet \rightarrow CH_3^\bullet + H_2O$ reaction can be calculated using heats of formation[53] or hydrogen atom bond dissociation energies[54] to give −14.5 and −14.8 kcal/mol, respectively. The G2 method[41,55] gives −13.5 kcal/mol for the enthalpy change of the forward reaction. At the UMP2 level the difference in ZP+thermal ($T = 298$ K) energy between reactants and products is 1.2 kcal/mol (Table 3), being smaller for the products. Therefore, for comparison to experiment, the calculated electronic energy difference between R and P has to be corrected by this amount. The adjusted exothermicities for this reaction are then −15.7, −15.7, and −11.1 kcal/mol for UMP2, PMP2, and CCSD(T), respectively. The ZP+thermal ($T = 298$ K) energy difference correction for DFT(B3LYP) is 0.9 kcal/mol (Table 4), to give a calculated reaction enthalpy of −11.9 kcal/mol. Again, PMP2 gives the closest result to experiment of these theory levels.

(4) $NH_3 + NH_2^\bullet \rightarrow NH_2^\bullet + NH_3$. The lowest energy reaction complex for reaction 4, RC′(**4**), is not on the least motion reaction path. The calculated equilibrium NH_3···H−NH structure has C_s symmetry and prefers a hydrogen bond between a NH_2 hydrogen atom and the lone pair electrons on NH_3, where the other N−H bonds are in a *trans*-staggered conformation. This NH_3···H−NH preference is probably due to the greater nucleophilic character of the ammonia lone pair of electrons compared to NH_2, as judged by the 16 kcal/mol larger proton affinity of NH_3 over NH_2.[53] The N···N distance in RC′(**4**) is 3.293 Å (UMP2) or 3.282 Å (DFT) and the N−H···N bridging angle is 166.0° (UMP2) or 170.2° (DFT). At both theory levels the unpaired spin density is concentrated on the amine nitrogen atom in the direction perpendicular to the molecular plane. Thus, as can be learned also from Table 5, the RC′(**4**) geometric structures calculated by UMP2 and DFT(B3LYP) are very similar. Unlike the reaction complexes discussed above that involved H atom abstraction from CH_4 and had electronic binding energies of less than 1 kcal/mol, the calculated electronic energy of RC(**9**) relative to reactants, shown in Table 2, ranges from −3.9 kcal/mol (UMP2, PMP2) to −3.6 kcal/mol (DFT). The unscaled ZP+thermal ($T = 298$ K) energy corrections here are 2.1 (UMP2) and 2.0 (DFT) kcal/mol, shown in Tables 3 and 4, respectively. These adjustments leave the net calculated binding energy of RC(**9**) in the range of 1.8−1.6 kcal/mol at room temperature. The unscaled ZPE differences alone are 1.7 (UMP2) and 1.6 (DFT) kcal/mol, so that at low temperature the calculated complex binding energy ranges from 2.2 to 2.0 kcal/mol.

Another reaction complex, RC(**4**), was found that does correspond to an incipient hydrogen atom transfer from NH_3 to NH_2 on the least motion reaction path, NH_2−H···NH_2. Both the UMP2 and DFT structures have C_s symmetry in a *trans* conformation, shown in Figure 4. Each structure shows all real frequencies in a harmonic force field calculation at its respective theory level. The electronic binding energies are 1.0 [UMP2, PMP2, CCSD(T)] or 1.2 (DFT) kcal/mol smaller than for RC′(**4**). Adding only the ZPE difference correction, as discussed above, leaves net binding energies ranging from 1.2 kcal/mol (UMP2) down to 0.8 kcal/mol at the DFT theory level for RC(**4**). As shown in Tables 3 and 4, the geometric parameters for the UMP2 and DFT RC(**4**) structures are similar in the H···N and N···N distances. Table 5 shows the same result for the angles. As also found for the geometric structures of the weak complexes discussed above, the bridging hydrogen bonds in both RC′(**4**) and RC(**4**) are usually more linear at the DFT than at the UMP2 level. Also like RC′(**4**), the unpaired spin density in RC(**4**) is localized mainly on the amine nitrogen atom (Tables 6 and 7) in the a″ direction.

The transition state structure, TS(**4**), has C_s symmetry and eclipsed N−H bonds above and below the plane. The UMP2 and DFT optimized geometries are similar, with H···N distances (1.230 and 1.250 Å) and N···H···N angles (153.6° and 157.6°) that are close. The one-dimensional symmetric optimization at the CCSD(T) level gives an energy minimum for a N···H distance of 2.47 Å (Table 2), which coincides almost exactly with the DFT value. Previous work[40] produced a linear N···H···N arrangement and overall C_{2h} symmetry for the transition state of this reaction. A significant difference in the calculated TS properties between UMP2 and DFT is in the imaginary frequency which represents the asymmetric motion of the bridging hydrogen atom about its symmetric position. The UMP2 calculated frequency is only 269 cm^{-1} (Table 3), which is unusually small compared to the reaction path frequencies at the saddle point calculated for the other hydrogen atom abstraction reactions studied here. The DFT(B3LYP) calculated frequency at 1614 cm^{-1} (Table 4) seems more normal and is similar to a configuration interaction result.[40] The low asymmetric TS frequency at the UMP2 level may represent a tendency of the UMP2 method to prefer a localized, asymmetric TS, although no such structure was actually found. As will be discussed subsequently, at the ROMP2 theory level the symmetric Cl···H···Cl geometry is a minimum and not a TS, as is also found for the UMP2 F···H···F symmetric structure in the $HF + F^\bullet \rightarrow F^\bullet + HF$ reaction.[71] This latter aspect will be further discussed below with regard to HO···H···OH. The reason for the eclipsed NH_2···H···NH_2 geometry is not clear. Attempts to generate a fully staggered conformation TS using DFT

resulted in the initially positioned staggered form optimizing back to the eclipsed structure.

The barrier height for TS(**4**) has electronic energies of 13.2 (UMP2), 10.1 (PMP2), 12.5 [CCSD(T)], and 6.4 (DFT) kcal/mol relative to reactants. The ZP+thermal ($T = 298$ K) energy corrections are −0.5 (UMP2) and −0.8 (DFT) kcal/mol. The relatively large difference (∼3 kcal/mol) between the UMP2 and PMP2 results is a reflection of the larger $\langle \mathbf{S}^2 \rangle$ value of 0.7979 for TS(**4**) calculated at the UHF level (Table 3) compared to the TS of the other reactions discussed above. Under such circumstances, PMP2 can tend to overcompensate and give energy values that are too low.[6−9] A previous BEBO-like estimate[39a] of the barrier height for the $NH_3 + NH_2^\bullet \rightarrow NH_2^\bullet + NH_3$ reaction yielded a value of ∼17 kcal/mol.[40] In the absence of experimental data for comparison and based on the above discussion the best estimate for the transition state energy is that it lies in the range 9.5−12 kcal/mol. The DFT(B3LYP) calculated electronic barrier (6.4 kcal/mol), adjusted for ZP+thermal ($T = 298$ K) energy differences, is 5.6 kcal/mol. This barrier height is smaller than the PMP2 value and by comparison to the other theory levels also seems to be too low.

As also found for the other transition states studied here, TS(**4**) has its unpaired spin density localized along the N···H···N bonding axis. In contrast, both in RC′(**4**) and RC(**4**) the radical electron is located in an orbital perpendicular to the N−H···N axis. Likewise, the geometric conformations of both RC′(**4**) and RC(**4**), the latter which lies on the least motion reaction path, are very different from TS(**4**). Therefore, reaching the TS(**4**) structure from either of the reactant complex conformations requires substantial geometric and electronic rearrangements. These substantial changes could be contributing factors to the relatively large calculated barrier for the $NH_3 + NH_2^\bullet$ symmetric exchange reaction.

(5) $NH_3 + OH^\bullet \rightarrow NH_2^\bullet + H_2O$. Reaction 5 has been studied by several groups.[42,72−76] No DFT results have been reported. Experimentally, the forward reaction is exothermic by 11.4−11.9 kcal/mol.[53,54] The electronic energy differences between reactants and products in Table 1 ranges from −10.5 (UMP2) to −8.9 [CCSD(T)] kcal/mol. As shown in Tables 3 and 4, the ZP+thermal ($T = 298$ K) energy is larger in the reactants than in the products at both the UMP2 and DFT-(B3LYP) theory levels. Therefore, this addition raises the calculated electronic energy differences and brings them closer to experiment. The resultant adjusted exothermicities (Table 2) are 11.8 (UMP2), 11.9 (PMP2), 10.2 [CCSD(T)], and 10.3 (DFT) kcal/mol. The G2 method[41,55] gives 11.3 kcal/mol. The agreement with experiment at all theory levels is very good.

The most stable reaction complex is shown in Figure 5 [RC′(**5**)]. This weakly bound complex is not on the least motion reaction path. The calculated geometric structure shows that the NH_3···H−O interaction is more stabilizing than the reaction path NH_2−H···OH interaction. In fact, the proton affinity of NH_3 is much larger than that of OH,[53] indicating that NH_3 is more nucleophilic than OH and, perhaps, explaining the preferred geometric configuration of the global minimum reaction complex. The electronic energy of RC(**5**) relative to reactants is substantial, compared to the previously discussed reaction complexes in this study and amounts to −8.0 (UMP2, PMP2), −7.8 [CCSD(T)], and −8.3 (DFT) kcal/mol at the various theory levels. Adjusted for ZP+thermal ($T = 298$ K) energy differences of 2.4 (UMP2) or 2.1 (DFT) kcal/mol, the net calculated binding energies are 5.6, 5.4, and 6.2 kcal/mol, respectively. The relatively large adjustment energies, which are mostly ΔZPE, also reflect the relative strong binding effect. The optimized geometry of RC(**5**) has essentially C_{3v} symmetry with a near-linear N···H−O angle at both the UMP2 and DFT levels (Tables 3 and 4). The two structures differ only by ∼0.03 Å in the N···H distance, which also carries over to the N···O length. The atomic spin density populations also agree closely between the UMP2 and DFT wave functions (Tables 6 and 7). The unpaired spin is localized mainly on the oxygen atom in the π direction perpendicular to the symmetry reflection plane containing H−N···H−O. It should be noted that within C_{3v} symmetry this electronic state is a doubly degenerate $^2\Pi$ state. The calculations here, of course, give only one component of the Π state.

Another weakly bound reaction complex was found only at the DFT(B3LYP) level that looks somewhat like the least motion path NH_3···OH structure. This geometry is also shown in Figure 5 [RC(**5**)]. Here, two N−H bonds are interacting equivalently with the hydroxyl oxygen atom, where the third N−H bond and the O−H bond are in an eclipsed conformation in the C_s plane. The unpaired spin located mainly on the oxygen atom is localized approximately along the N···O axis. As shown in Table 4, both the H−N···O and N···O−H angles are close to 90°. The H−N···O−H dihedral angle is 0°. The DFT electronic binding energy relative to reactants for RC(**5**) is 5.2 kcal/mol, and 3.4 kcal/mol after adjustment for the ZPE difference with the products P. When initially positioned in or around the DFT optimized RC(**4**) geometry, the UMP2 optimization rotated to the more stable RC′(**5**). It may be necessary to carry out a more exhaustive search of the energy surface, including different spin doublet electronic states, to confirm that the global minimum has been found here for the NH_3···OH complex.

The measured activation energies for the $NH_3 + OH^\bullet \rightarrow NH_2^\bullet + H_2O$ reaction, as obtained from Arrehenius plots, are 4.1 kcal/mol at $T = 1000$ K[58] and 2.6 kcal/mol in the 273 K ≤ T ≤ 433 K range.[70,76] The calculated transition state energy for TS(**5**) relative to reactants is 8.9 (UMP2), 6.7 (PMP2), and 5.5 [CCSD(T)] kcal/mol. Adjusting these values by the ZP+thermal (298 K) energy difference of 1.4 kcal/mol from the UMP2 frequency calculation reduces the barrier height for the forward reaction to 7.5, 5.3, and 4.1 kcal/mol, respectively. In contrast however, as shown in Table 1, the electronic DFT(B3LYP) energy of TS(**5**) is below that of the reactants by 2.7 kcal/mol. There is also a 1.5 kcal/mol ZP+thermal ($T = 298$ K) energy difference between reactants and TS(**5**), shown in Table 4. With this adjustment TS(**5**) becomes 4.2 kcal/mol more stable than reactants (Table 2). Thus, the DFT(B3LYP) theory level predicts a negative transition state energy in the forward direction, R → P. The activation energy in the reverse reaction direction should be the sum of the endothermicity and forward activation energies, which experimentally is ∼14.2 kcal/mol (Table 2). There is almost no difference between P and TS(**5**) in the calculated ZP+thermal ($T = 298$ K) energy at both the UMP2 and DFT levels. Therefore, the reverse activation barriers remain essentially as calculated from the electronic energy differences, which are 19.4 (UMP2), 17.3 (PMP2), 14.4 [CCSD(T)], and 6.3 (DFT) kcal/mol. The DFT value here seems to seriously underestimate E_a in both the forward and reverse directions, while CCSD(T) gives a good accounting of both barrier energies.

Consistent with their very different calculated transition state energies, the UMP2 and DFT optimized geometric structures for TS(**5**), labeled TS(**5a**) and TS(**5b**), respectively in Tables 3, 4, 6, and 7, have somewhat different conformations. The UMP2 structure has the O−H bond close to bisecting the NH_2 angle. Thus, the H−N···O−H dihedral angles (ignoring the intervening hydrogen atom) are 67.5° and −41.5°. In contrast,

the DFT geometry has an essentially eclipsed O−H and N−H bond configuration, with H−N···O−H angles of 2.3° and 107.9°. The UMP2 and DFT structures also differ in the bond lengths involving the bridging hydrogen atom. At the UMP2 level the N···H distance at 1.110 Å is much shorter than the 1.312 Å H···O distance (Table 3), as befits the expectation of an early transition state for an exothermic reaction. The DFT transition state (Table 4) has a shorter H···O length and a longer N···H bond, both by ∼0.04 Å. As has been found here generally, but not always, the one-dimensional CCSD(T) optimization of the TS structure (Table 3) brings the N···H and H···O distances closer to the DFT values. The atomic spin density populations at the TS reflect these geometric structure differences. The UMP2 radical electron (Table 6) is located much more on oxygen than on nitrogen, while at the DFT level the spin populations are more equal. In both cases the unpaired spin is mainly along the N···H···O axis. The N···O distance, however, is similar in the two methods. The bond angles involving the remote hydrogen atoms (Table 5) are also close to each other in the two structures. In all, despite different H−N···O−H orientations, the H−N···H···O conformations are similar with dihedral angles of 53.4° and −61.8° (UMP2) and 64.1° and −67.7° (DFT) for the two amine hydrogen atoms. Starting with the DFT TS(**5b**) geometry and doing a UMP2 saddle point geometry optimization leads back to TS(**5a**). Analogously, starting with the TS(**5a**) structure and DFT geometry optimizing for a transition state leads back to the TS(**5b**) form.

Because of the difference in geometric configuration between the UMP2 TS(**5a**) and DFT TS(**5b**) conformations, direct CCSD(T) geometry optimization using numerically estimated gradients was carried out on the NH_2···H···OH transition state starting from the UMP2 structure. Converged geometry results show that the initial staggered configuration has rotated to the eclipsed DFT conformation, with N···H and H···O distances of 1.14 and 1.29 Å, respectively. The eigenvalues of the final Hessian show one large negative value, indicative of a transition state. The CCSD(T) electronic energy translates into a E_a value of ∼3.9 kcal/mol, compared to 4.1 kcal/mol at the UMP2 geometry and 4.2 kcal/mol for the IRC(UMP2) interpolated energy (Table 2). The CCSD(T) optimized N···H and H···O distances agree very well with the IRC(UMP2) interpolated values and are halfway between the UMP2 and DFT optimized bond lengths (Tables 3 and 4). Thus, the DFT(B3LYP) optimized transition state geometry is reliable, perhaps even more so than UMP2, even though giving poor energetics by predicting a negative activation energy for this reaction.

The product complex, PC(**5**), corresponding to the reaction path NH_2···H−OH hydrogen-bonded complex, is also found in two forms, shown as PC(**5a**) and PC(**5b**). The UMP2 form, (**5a**), has C_s symmetry with the two N−H bonds located symmetrically above and below the plane. The DFT(B3LYP) structure, PC(**5b**), also has a reflection plane which contains all the atoms in the complex. PC(**5a**) and PC(**5b**) differ by a 90° rotation of the NH_2 group about the H···N axis. All the frequencies in both PC(**5**) structures are real, showing that the two different conformers are minima, each at its respective theory level. Starting with the PC(**5b**) conformation and gradient optimizing the geometry at the UMP2 theory level gives a stationary PC(**5b**) structure that has one imaginary frequency corresponding to the NH_2 rotation toward the (**5a**) conformer. Analogously, starting with the PC(**5a**) form and DFT(B3LYP) optimizing the geometry gives a saddle point PC(**5a**) structure. Thus, PC(**5a**) is the global energy minimum at the UMP2 level, and PC(**5b**) is the global energy minimum at the DFT(B3LYP) level. Each method has the other method's equilibrium geometry as a transition state in the rotational motion of the NH_2 group. The rotation barrier height in each case is less than 0.05 kcal/mol. The unpaired spin density in PC(**5**) is located along the N···H−O axis, mainly on the nitrogen atom (Tables 6 and 7) in both (**5a**) and (**5b**), both for the energy minima and for the rotamer transition states. In the following discussions, PC(**5**) refers to (**5a**) for the UMP2-based methods and (**5b**) for the DFT theory level.

The product complex, PC(**5**), corresponding to the exit channel NH_2···H−OH interaction, is predicted to be bound. The electronic stabilization relative to products is 5.6 (UMP2, PMP2), 5.4 [CCSD(T)], and 5.3 (DFT) kcal/mol. The ZP+thermal (T = 298 K) energy difference between PC(**5**) and P is 2.3 kcal/mol at both the UMP2 and DFT theory levels. The adjusted PC(**5**) binding energies are, therefore, 3.3 (UMP2, PMP2), 3.1 [CCSD(T)], and 3.0 (DFT) kcal/mol. For PC(**5**) DFT theory level gives a dissociation energy that is very similar to the other *ab initio* methods. However, as noted, the conformations of the UMP2 and DFT geometric structures are different. At the UMP2 level the H−N···H−O dihedral angles in PC(**5**) are 82.3° and −82.6°. The DFT optimized geometry has the two NH_2 bonds coplanar with the other atoms, with H−N···H−O dihedral angles of 0° and 179.9°. The other structural parameters are similar between the two conformations (Tables 3−5). Given the miniscule energy difference between PC(**5a**) and PC(**5b**) at both the UMP2 and DFT(B3LYP) levels, the question of the correct conformation of PC(**5**) was not pursued further.

The energetics and stationary points for the $NH_3 + OH^\bullet \rightarrow NH_2^\bullet + H_2O$ reaction have been studied theoretically,[40,72−75] with geometry optimizations mainly at the MP2 level in a 6-31G(d,p) basis set and higher level theory single-point calculations. For the geometry of the TS both the staggered[72,73] and eclipsed[74,75] forms have been found. The most recent results[72] show the N−H distance to be ∼1.1 Å and the H···O distance to be ∼1.3 Å in the TS, which is similar to that found here (Tables 3 and 4). Previous calculated activation energies have ranged from 1.0 to 5.9[72,75] kcal/mol, and the reaction energy for the same set of methods ranges from −11.8 to −13.3 kcal/mol.[72] The best energy results have been obtained at the QCISD(T)//MP2 level,[80] which is similar to CCSD(T)[11] but less comprehensive.[81] A reaction path complex, NH_2−H···OH, was UMP2/6-31G(d,p) located having a *cis*, staggered conformation and an electronic energy between −0.3 and −0.6 kcal/mol[72] relative to reactants. This UMP2 analogue to RC(**5**) was not found here with the better basis set. The NH_2···H−OH product complex, with a *trans*, staggered form, has been found to be bound relative to reactants by 12.3−14.5 kcal/mol.[72,74] These latter energies are very similar to the corresponding quantities calculated here (Table 2).

(6) $H_2O + OH^\bullet \rightarrow OH^\bullet + H_2O$. Aspects of identity exchange reaction 6 have been studied both theoretically[40,77,78] and experimentally.[79] There are no reported DFT calculations on this system. Two weakly bound H_2O···OH complexes have been identified[77−79] in this study. The first, the more loosely bound RC(**6**), lies on the least motion reaction path and has a planar HO−H···OH structure, with the radical electron on the hydroxyl oxygen atom in the out-of-plane a″ direction. RC(**6**) was obtained here only at the UMP2 level. All attempts to generate the RC(**6**) structure with DFT(B3LYP) resulted in the RC′(**6**) geometric configuration. The second, more strongly bound complex, RC′(**6**), shows a H_2O···H−O geometry and is found at both the UMP2 and DFT(B3LYP) theory levels. This geometric preference is probably due to the water molecule

being more nucleophilic than the hydroxyl radical. RC′(**6**) has a bent OH_2 group and a $^2A'$ electronic state in C_s symmetry, where the unpaired electron is in a hydroxyl π orbital perpendicular to the >O···H−O axis.

The electronic binding energy (Table 2) of RC(**6**) is calculated to be 3.7 [UMP2, PMP2, and CCSD(T)] kcal/mol. The ZP+thermal (T = 298 K) energy correction is 1.7 kcal/mol (Table 3) so that the net binding energy for RC(**6**) is 2.0 kcal/mol at all the UMP2-based levels. The (water)H···O distance for this complex is 2.100 Å for the UMP2 structure, which is similar to the highest level calculational result reported previously.[78a] The (water)H···OH angle is calculated here to be 100.3° (Table 5), also similar to, but smaller than, that found by others.[78b] The more stable hydrogen-bonded complex, RC′(**6**), is 6.4 (UMP2 and PMP2) or 6.3 [CCSD(T)] and DFT] kcal/mol more stable than reactants. After a ZP+thermal (T = 298 K) energy adjustment of 2.0 kcal/mol (UMP2 and DFT) the net binding energy is 4.4 (UMP2 and PMP2) or 4.3 [CCSD(T) and DFT] kcal/mol. Thus, the stabilization energies at all the levels are very similar. The (HO)H···O distance in RC′(**6**) is found to be 1.927 Å (UMP2) or 1.891 Å (DFT). These bond length values are also somewhat shorter than reported previously for the same conformation.[78b] A comprehensive study of hydrogen bonding between H_2O and $OH^•$ has been carried out by Schaefer *et al.*[78]

The HO···H···OH transition state has been studied in detail.[40,77,79] All results or assumptions have centered about a symmetric structure for the TS. However, no unconstrained geometry optimization has been reported. The UMP2 calculated TS geometry, TS(**6**), turns out to have an asymmetric geometric structure with O···H and H···O bond lengths of 1.110 and 1.199 Å, respectively (Table 3). A harmonic force field analysis of TS(**6**) shows one imaginary frequency of 2475 cm^{-1}, corresponding to the antisymmetric motion of the bridging hydrogen atom along the bonding axis. The terminal O−H bonds are in almost perpendicular planes to each other with a H−O···O−H dihedral angle of 113.4°, while the O···H···O angle is 141.9°. In projection along the O···O axis the three hydrogen atoms are equidistant. An asymmetric transition state at the restricted open MP2 level has also been found for the valence isoelectronic Cl···H···Cl system,[71b] which, however, becomes a symmetric TS with UMP2. However, for the F···H···F transition state of the HF + $F^•$ → $F^•$ + HF reaction the UMP2/6-31G(d,p) level of calculation predicts the symmetric structure to be an energy minimum, bracketed by two asymmetric structure saddle points.[71a] The analogous result is obtained here at the UMP2 level for the isoelectronic HO···H···OH transition state, where the symmetric structure, SS(**6**) (see TS structure in Figure 6), is an energy minimum with equivalent O···H distances of 1.166 Å and all real frequencies. UMP2 SS(**6**) has C_2 symmetry with a H−O···O−H dihedral angle of 115.3°. The O···H···O angle in SS(**6**) is 140.7° (Table 3).

In contrast, the DFT(B3LYP) method finds SS(**6**) to be the transition state for the H_2O + $OH^•$ → $OH^•$ + H_2O reaction with an imaginary frequency of 1474 cm^{-1} (Table 4), corresponding to the asymmetric stretch of the bridging hydrogen atom. In the DFT SS(**6**) geometry, the O···H distances are 1.166 Å, the O···H···O angle is 145.7, and the H−O···O−H dihedral angle is 122.2°. The H−O···H angle for all three geometric structures [TS(**6**) and both the UMP2 and DFT SS(**6**)] is in the 103−105° range, as shown in Table 5. In summary, all three structures, whether symmetric or asymmetric, have qualitatively similar geometric parameters. Analogously, the unpaired spin density in all three structures is concentrated on the oxygen atoms along the O···H···O axis.

The asymmetric UMP2 transition state describes a H_2O + $OH^•$ → $OH^•$ + H_2O reaction path having a double-humped maximum and an intervening minimum at the symmetric geometry. No evidence of such a structure has been found in the recent experimental study of HO···H···OH by photoelectron spectroscopy of the anion.[79] After applying the 1.1 kcal/mol ZP+thermal (T = 298 K) correction (Table 3) to the electronic energy difference, the 10.9 kcal/mol UMP2 E_a calculated at the TS(**6**) saddle point geometry (Table 2) is much above the estimated experimental value of 5.3 kcal/mol,[77] even if the calculated activation energy is expected to be larger than the fitted Arrehenius activation energy. CCSD(T)//UMP2 corrects, somewhat, for the UMP2 overestimation, and the activation barrier energy relative to reactants decreases to 8.7 kcal/mol. Altogether, the UMP2 result seems to give the wrong geometric configuration for the TS and too high a saddle point energy. The DFT calculated electronic barrier height energy of 1.3 kcal/mol with a symmetric SS(**6**) structure is certainly too low compared to experiment. If the 1.3 kcal/mol ZP+thermal (T = 298 K) energy differential (Table 4) is subtracted from this value, then the DFT activation energy is effectively reduced to zero.

The symmetric nature of the HO···H···OH transition state was confirmed by reoptimization at the CCSD(T) and CAS(7,7)-MCSCF[82] theory levels. Both methods give a symmetric transition state, in agreement with the DFT(B3LYP) result. The CCSD(T) optimized O−H distances are 1.164 Å, in exact agreement with the one-dimensional CCSD(T) scaling procedure (Table 3) and with the DFT bond lengths (Table 4). The O−H−O angle is 142.2° and the H−O···O−H dihedral angle is 118.7°. The barrier height energy increases by 0.2 kcal/mol relative to CCSD(T)//UMP2 to a calculated E_a of 8.9 kcal/mol. The eigenvalue spectrum of the CCSD(T) updated Hessian matrix shows one negative value corresponding to the asymmetric motion of the bridging hydrogen atom. Although this is not exactly the same as direct harmonic force field analysis, which was too difficult to carry out, the negative eigenvalue is large enough to establish the CCSD(T) optimized symmetric structure as a transition state.

The CAS(7,7)−MCSCF method mixes all electron configurations arising from the distribution of seven electrons among seven molecular orbitals (MOs) to define the active space. This leaves a passive space of six doubly occupied MOs that are not correlated in the wave function. The passive space consists of the oxygen 1s and 2s and O−H bonding orbitals for each oxygen atom. The resultant optimized CAS(7,7) TS geometry has O···H distances of 1.176 Å and an O···H···O angle of 144.5°. The saddle point frequency, obtained from a harmonic force field analysis, is 3228 cm^{-1}, which is much larger than the DFT frequency for SS(**6**) in Table 4. Given the low DFT barrier height, a low saddle point frequency is not unexpected.

In the F···H···F case, previous work has shown that both the CCSD(T) and CAS methods give a symmetric transition state, unlike the UMP2 asymmetric TS.[71a] The DFT(B3LYP)/6-311++G(2d,p) transition state structure was, therefore, also calculated here for the HF + $F^•$ reaction. The result is another symmetric TS with 1.10 Å F···H distances and a F···H···F angle of 138.3°. These values are typical of the higher theory level results for these parameters.[71a] The DFT saddle point frequency is calculated to be only 1499 cm^{-1}, which, again, is low compared to other high-level methods.[71a] Thus, at the UMP2 level the F···H···F and HO···H···OH transition states are asymmetric, NH_2···H···NH_2 is symmetric but shows signs of incipient symmetry breaking, and CH_3···H···CH_3 is calculated to be symmetric with a reasonable transition state frequency.

DFT(B3LYP) correctly predicts all these TS to be symmetric with geometric parameters that are close to high-level theory values, but with smaller saddle point frequencies.

4. Summary

Ab initio electronic structure calculations have been carried out on six hydrogen abstraction reactions. Geometric structures for the reactants, reactant complexes, transition states, product complexes, and products have been gradient optimized at both the UMP2 and DFT(B3LYP) theory levels using the 6-311++G(2d,p) basis set. The character of each stationary state as a minimum or a saddle point was determined by the number of imaginary frequencies in a harmonic force field calculation. PMP2 and CCSD(T) energies were also calculated at the UMP2 optimized geometries. The reaction energies and barrier heights were compared with experiment, where possible. Geometric structures and wave function and energy properties have been compared between the UMP2-based and DFT(B3LYP) methods.

Reaction energies are, perhaps, the simplest and most straightforward property to compare among the different theory models and with experiment. In general, for the three asymmetric reactions, the (absolute value) UMP2 and PMP2//UMP2 results are on the high side or even slightly above the experimental range, while CCSD(T)//UMP2 and DFT are on the low side or somewhat below experiment. G2[41,55] calculated exothermicities fall between these two trends. In all three cases the DFT reaction energies are within 1.6 kcal/mol of the G2 result, but smaller in magnitude. The good performance of DFT(B3LYP) in calculating reaction energies has been noted previously.[17]

Activation barriers are more difficult to compare with experiment since they are not measured directly. The calculated E_a values are expected to be somewhat larger than the Arrehenius fitted experimental energies; but it is not known by how much. The UMP2, PMP2//UMP2, and CCSD(T)//UMP2 methods give activation energies that are somewhat greater than the Arrehenius values, as expected. Experience to date[18,27,28,30−37] indicates that although the hybrid functional is the most promising DFT method, it tends to underestimate reaction barrier heights. The results obtained here tend to partially confirm this assessment. The DFT(B3LYP) calculated activation energies are the smallest of all the theory levels tested here for each reaction and are roughly equal to, or less than, the corresponding Arrehenius barriers. The degree that DFT(B3LYP) underestimates E_a seems to increase with the electronegativity of the atoms X and Y involved in the reaction; O > N > C. Thus, for the $CH_4 + CH_3$ reaction DFT(B3LYP) predicts an activation barrier close to the Arrehenius E_a, and the comparison gets worse from there as X and/or Y become more electronegative. These observations are consistent with the recent success of Houk *et al.*[83] and others[30c,36b] in calculating hybrid functional DFT activation barriers in hydrocarbon reactions.

Despite sometimes poor activation energies, the geometric and electronic structure properties of the three exchange reaction transition states are generally very similar between the UMP2 and DFT(B3LYP) methods. Since the DFT calculated exothermicity is usually smaller than for UMP2, the DFT TS geometry is usually found later along the reaction path (i.e., longer X···H and shorter H···Y). The unpaired spin density populations also follow these trends with larger values on X and lower values on Y on going from the UMP2 to the DFT(B3LYP) transition state for a given reaction. For these exchange reactions one-dimensional CCSD(T) optimization of each TS geometry using the UMP2 level IRC points results in X···H and H···Y distances that are generally closer to the DFT(B3LYP) geometric parameters. This result is expected on the basis of the calculated CCSD(T) exothermicities. However, the improved agreement is also found for scaling the X···H distances in the TS of the identity reactions.

For the identity reactions symmetric transition states are expected. Here, DFT(B3LYP) performs better than UMP2. For the $NH_3 + NH_2$ reaction the UMP2 imaginary frequency at the TS, which delineates the reaction path direction connecting reactants and products, is abnormally small, indicative of an incipient symmetry-breaking instability. The DFT(B3LYP) calculated frequency is reasonable. For $H_2O + OH^•$ the UMP2 transition state is predicted to be asymmetric, with the symmetric structure being an energy minimum. The DFT(B3LYP) method correctly predicts a symmetric geometry for this identity reaction. Direct CCSD(T) and CAS(7,7)-MCSCF geometry optimizations of the TS confirm the symmetric nature of HO···H···OH. Also, contrary to UMP2, DFT(B3LYP) correctly gives a symmetric F···H···F transition state geometry.

For the weakly bonded reaction and product complexes UMP2 usually gives a larger binding energy than DFT(B3LYP), which for the weakest cases shows no energy minimum structure. In general, UMP2 probably overestimates complex binding because of BSSE, and DFT(B3LYP) underestimates dispersion energies.[47] For the hydrogen-bonded complexes, DFT(B3LYP) gives binding energies similar to CCSD(T)//UMP2 and smaller than the UMP2 values. Thus, DFT(B3LYP) seems to give good hydrogen bond energies for these radical species. For the hydroge-bonded complexes, the geometric structures at the DFT(B3LYP) and UMP2 levels generally agree very well. However, for both the $NH_3 + OH^•$ product complex and transition state there are differences in conformation between the UMP2 and DFT(B3LYP) structures. Direct CCSD(T) optimization confirms the DFT structure for the TS. The results obtained here for the hydrogen-bonded complexes and the transition states generally support the use of DFT(B3LYP) for geometric structure determination in a wide range of contexts.[84]

References and Notes

(1) (a) For a general overview of high-level *ab initio* methods see: Raghavachari, K.; Anderson, J. B. *J. Chem. Phys.* **1996**, *100*, 12960. Schlegel, H. B. *Adv. Chem. Phys.* **1987**, *67*, 249.

(2) Moller, C.; Plesset, M. S. *Phys. Rev.* **1934**, *46*, 618.

(3) Hehre, W. J.; Radom, L.; Schleyer, P. v. R.; Pople, J. A. *An Initio Molecular Orbital Theory*; J. Wiley & Sons: New York, 1986.

(4) Handy, N. C.; Knowles, P. J.; Somasundram, K. *Theor. Chim. Acta* **1985**, *68*, 87. Gill, P. M. W.; Radom, L. *Chem. Phys. Lett.* **1986**, *132*, 16. Nobes, R. H.; Pople, J. A.; Radom, L.; Handy, N. C.; Knowles, P. J. *Chem. Phys. Lett.* **1987**, *138*, 481.

(5) Durant, J. L., Jr.; Rohlfing, C. M. *J. Chem. Phys.* **1993**, *98*, 8031.

(6) Schlegel, H. B. *J. Chem. Phys.* **1986**, *84*, 4530. Schlegel, H. B.; Sosa, C. *Chem. Phys. Lett.* **1988**, *145*, 329. Schlegel, H. B. *J. Phys. Chem.* **1988**, *92*, 3075.

(7) Handy, N. C.; Su, M.-D.; Coffin, J.; Amos, R. D. *J. Chem. Phys.* **1990**, *93*, 4123.

(8) Gonzales, C.; Theisen, J.; Schlegel, H. B.; Hase, W. L.; Kaiser, E. W. *J. Phys. Chem.* **1992**, *96*, 1767.

(9) Chen, W.; Schlegel, H. B. *J. Chem. Phys.* **1994**, *101*, 5957.

(10) Bartlett, R. *J. Annu. Rev. Phys. Chem.* **1981**, *32*, 359; *J. Phys. Chem.* **1989**, *93*, 1697. Bartlett, R. J.; Stanton, J. F. *Rev. Comput. Chem.* **1994**, *5*, 65.

(11) Raghavachari, K.; Trucks, G. W.; Pople, J. A.; Head-Gordon, M. *Chem. Phys. Lett.* **1989**, *157*, 479. Stanton, J. F. *J. Chem. Phys.* **1994**, *101*, 37.

(12) Raghavachari, K.; Trucks, G. W.; Pople, J. A.; Head-Gordon, M. *Chem. Phys. Lett.* **1989**, *157*, 479.

(13) Ziegler, T. *Chem. Rev.* **1991**, *91*, 65l.

(14) Handy, N. C.; Tozer, D. J.; Laming, G. J.; Murray, C. W.; Amos, R. D. *Isr. J. Chem.* **1993**, *33*, 331.

(15) Kohn, W.; Becke, A. D.; Parr, R. G. *J. Phys. Chem.* **1996**, *100*, 12974.

(16) Johnson, B. G.; Gill, P. M.; Pople, J. A. *J. Chem. Phys.* **1993**, *98*, 5612.

(17) Becke, A. D. *J. Chem. Phys.* **1993**, *98*, 5648.

(18) Baker, J.; Muir, M.; Andzelm, J. *J. Chem. Phys*. **1995**, *102*, 2063.
(19) Baker, J.; Scheiner, A.; Andzelm, J. *Chem. Phys. Lett*. **1993**, *216*, 380. Laming, G. J.; Handy, N. C.; Amos, R. D. *Mol. Phys*. **1993**, *80*, 1121.
(20) Johnson, B. G.; Gonzales, C. A.; Gill, P. M. W.; Pople, J. A. *Chem. Phys. Lett*. **1994**, *221*, 100.
(21) (a) Han, W.-G.; Suhai, S. *J. Phys. Chem*. **1996**, *100*, 3942. (b) Del Bene, J. E.; Person, W. B.; Szczepaniak, K. *J. Phys. Chem*. **1995**, *99*, 1075. Sule, P.; Nagy, A. *J. Chem. Phys.* **1996**, *104*, 8524.
(22) Hay, P. J. *J. Phys. Chem*. **1996**, *100*, 5.
(23) Fan, L.; Ziegler, T. *J. Am. Chem. Soc*. **1992**, *114*, 10890.
(24) (a) Pederson, M. R. *Chem. Phys. Lett*. **1994**, *230*, 554. (b) Porezag, D.; Pederson, M. R. *J. Chem. Phys*. **1995**, *102*, 9345.
(25) Fox, G. L.; Schlegel, H. B. *J. Phys. Chem*. **1992**, *96*, 298.
(26) (a) Jursic, B. S. *Chem. Phys. Lett.* **1995**, *244*, 263. (b) Jursic, B. S. *Chem. Phys. Lett*. **1996**, *256*, 603. (c) Jursic, B. S.; Zdravkovski, Z. *J. Chem. Soc., Perkin Trans*. **1995**, *2*, 1223.
(27) Stanton, R. V.; Merz, K. M., Jr. *J. Chem. Phys.* **1994**, *100*, 434.
(28) Deng, L.; Ziegler, T. *Int. J. Quantum. Chem*. **1994**, *52*, 731.
(29) Green, W. H. *Int. J. Quantum. Chem*. **1994**, *52*, 837.
(30) Baker, J.; Andzelm, J.; Muir, M.; Taylor, P. R. *Chem. Phys. Lett*. **1995**, *237*, 53.
(31) Durant, J. L. *Chem. Phys. Lett*. **1996**, *256*, 595.
(32) (a) Sosa, C.; Lee, C. *J. Chem. Phys*. **1993**, *98*, 8004. (b) Carpenter, J. E.; Sosa, C. P. *J. Mol. Struct. (THEOCHEM)* **1994**, *311*, 325.
(33) Barone, V.; Orlandini, L. *Chem. Phys. Lett*. **1995**, *246*, 45.
(34) Nachtigall, P.; Jordan, K. D.; Smith, A.; Jonsson, H. *J. Chem. Phys.* **1996**, *104*, 148.
(35) Oie, T.; Topol, I. A.; Burt, S. K. *J. Phys. Chem*. **1995**, *99*, 905.
(36) Melius, C. F. In *Chemistry and Physics of Energetic Materials*; Bulusu, S. N., Ed.; Kluwer Academic Press: Dordrecht. 1990.
(37) (a) Johnston, H. S. *Gas Phase Reaction Theory*; Ronald Press: New York, 1966. Laidler, K. J. *Chemical Kinetics*, 3rd ed.; Harper & Row: New York. 1987. (b) Hoz, S. *Acc. Chem. Res*. **1993**, *26*, 69.
(38) Williams, I. H. *Chem. Soc. Rev.* **1993**, 277.
(39) (a) Zavitsas, A. A. *J. Am. Chem. Soc*. **1972**, *94*, 2779. Roberts, B. P.; Steel, A. J. *J. Chem. Soc., Perkin Trans*. **1994**, *2*, 2155. (b) Shaik, S.; Reddy, A. *J. Chem. Soc., Faraday Trans*. **1994**, *90*, 1631.
(40) Leroy, G.; Sana, M.; Tinant, A. *Can. J. Chem*. **1985**, *63*, 1447. Sana, M.; Leroy, G.; Villaveces, J. L. *Theor. Chim. Acta* **1984**, *65*, 109.
(41) Frisch, M. J.; *et al*. *Gaussian 9*4, Gaussian, Inc.: Pittsburgh, PA, 1995.
(42) Stephens, P. J.; Devlin, F. J.; Chabalowski, C. F.; Frisch, M. J. *J. Phys. Chem*. **1994**, *98*, 11623.
(43) Gonzales, C.; Schlegel, H. B. *J. Chem. Phys*. **1990**, *94*, 5523.
(44) Espinosa-Garcia, J.; Orchado, J. C. *J. Phys. Chem*. **1995**, *99*, 8613.
(45) Boys, S. F.; Bernardi, F. *Mol. Phys*. **1970**, *19*, 553.
(46) Basch, H. *Inorg. Chim. Acta* **1996**, *242*, 191.
(47) (a) Perez-Jorda, J. M.; Becke, A. D. *Chem. Phys. Lett*. **1995**, *134*, 233. (b) Kristyan, S.; Pulay, P. *Chem. Phys. Lett.* **1994**, *229*, 175. (c) Lundqvist, B. I.; Andersson, Y.; Shao H.; Chan, S.; Langreth, D. C. *Int. J. Quantum. Chem*. **1995**, *56*, 247.
(48) Wiberg, K. B.; Hadad, C. M.; LePage, T. J.; Breneman, C. M.; Frisch, M. J. *J. Am. Chem. Soc*. **1992**, *96*, 671.
(49) (a) Chandra, A. K. Malar, E. J.; Gupta, D. S. *Int J. Quantum. Chem*. **1992**, *41*, 371. (b) Chandra, A. K.; Rao, V. S. *Int. J. Quantum. Chem*. **1993**, *47*, 437. (c) Wildman, T. A. *Chem. Phys. Lett*. **1986**, *126*, 325.
(50) Chen, Y.; Tschuikov-Roux, E. *J. Phys. Chem*. **1993**, *97*, 3742.
(51) Litivinowicz, J. A.; Ewing, D. E.; Jurisevic, S.; Manka, M. J. *J. Phys. Chem*. **1995**, *99*, 9709.
(52) *CRC Handbook of Bimolecular and Termolecular Gas Reactions*; Kerr, J. A., Moss, S. J., Eds.; CRC Press: Boca Raton, FL 1981; Vol. 1.
(53) (a) Lias, S. G.; Bartmess, J. E.; Liebman, J. F.; Holmes, J. L.; Levin, R. D.; Mallard, W. G. *J. Phys. Chem. Ref. Data*, *17*, **1988**, Suppl. 1. (b) *CRC Handbook of Chemistry and Physics*, 74th ed.; Lide, D. R., Ed.; CRC: Boca Raton, FL, 1995−6.
(54) Berkowitz, J.; Ellison, G. B.; D. Gutman, D. *J. Phys. Chem*. **1994**, *98*, 2744.
(55) Curtiss, L. A.; Raghvachari, K.; Trucks, G. W.; Pople, J. A *J. Chem. Phys*. **1991**, *94*, 7221.
(56) Hammond, G. S. *J. Am. Chem Soc.* **1955**, *77*, 334.
(57) (a) Hennig, G.; Wagner, H. Gg. *Ber. Bunsen-Ges. Phys. Chem*. **1995**, *99*, 863. (b) Hack, W.; Kurzke, H.; Rouveirolles, P. Wagner, H. G. *Proc Int. Sym. Combust*. **1986**, *21*, 905, *Chem. Abstr*. **1988**, *109*, 210466b.
(58) Green, W. H. Private communication.
(59) Demissy, M.; R. Lesclaux, R. *J. Am. Chem. Soc*. **1980**, *102*, 2898.
(60) Gonzales, C.; McDougall, J. J. W.; Schlegel, H. B. *J. Phys. Chem*. **1990**, *94*, 7467.
(61) Dobbs, K. D.; Dixon, D. A.; Komornicki, A. *J. Chem. Phys*. **1993**, *98*, 8852.
(62) Bottini, A.; Poggi, G.; Emmi, S. S. *J. Mol. Struct. (THEOCHEM*) **1993**, *279*, 299.
(63) (a) Melissas, V. S.; Truhlar, D. G. *J. Phys. Chem*. **1994**, *98*, 875. (b) Melissas, V. S.; Truhlar, D. G. *J. Chem. Phys*. **1993**, *99*, 1013.
(64) Jones, S. A. L.; Pacey, P. D. *J. Phys. Chem*. **1992**, *96*, 1764.
(65) Melissas, V. S.; Truhlar, D. G. *J. Chem. Phys.* **1993**, *99*, 3542.
(66) Hu, W.-P.; Liu, Y.-P.; Truhlar, D. G. *J. Chem. Faraday Trans.* **1994**, *90*, 1715.
(67) Nyman, G.; Clary, D. C. *J. Chem. Phys*. **1994**, *101*, 5756.
(68) De More, W. B. *J. Phys. Chem*. **1993**, *97*, 8564.
(69) Dunlop, J. R.; Tully, F. P. *J. Phys. Chem*. **1993**, *97*, 1148.
(70) Atkinson, R.; Baulch, D. L. Cox, R. A.; Hampson, R. F., Jr.; Kerr, J. A.; Troe, J. *J. Phys. Chem. Ref. Data* **1989**, *18*, 881.
(71) (a) Fox, G. L.; Schlegel, H. B. *J. Am. Chem Soc*. **1993**, *115*, 6870. (b) Visscer, L.; Dyall, K. G. *Chem. Phys. Lett*. **1995**, *239*, 181.
(72) Corchado, J. C.; Olivares del Valle, F. J.; Espinosa-Garcia, J. *J. Phys. Chem*. **1993**, *97*, 9129.
(73) Espinosa-Garcia, J.; Ojalvo, E. A.; Corchado, J. C. *J. Mol. Struct. (THEOCHEM*) **1994**, *303*, 131.
(74) Espinosa-Garcia, J.; Corchado, J. C. *J. Chem. Phys*. **1994**, *101*, 8700.
(75) Gimenez, X.; Moreno, M.; Lluch, J. M. *Chem. Phys*. **1992**, *165*, 41.
(76) Diau, E. W.-G.; Tso, T.-L.; Lee, Y.-P. *J. Phys. Chem*. **1990**, *94*, 5261.
(77) Nanayakkara, A. A.; Balint-Kurti, G. G.; Williams, I. H. *J. Phys. Chem*. **1992**, *96*, 3662.
(78) (a) Kim, K. S.; Kim, H. S.; Jang, J. H.; Kim, H. S.; Mhin, B.-J.; Xie, Y.; Schaefer, H. F., III. *J. Chem. Phys*. **1991**, *94*, 2057. (b). Xie, Y.; Schaeffer, H. F., III. *J. Chem. Phys*. **1993**, *98*, 8829.
(79) Arnold, D. W.; Xu, C.; Neumark, D. M. *J. Chem. Phys*. **1995**,*102*, 6088.
(80) Pople, J. A.; Head-Gordon, M.; Raghavachari, K. *J. Chem. Phys*. **1987**, *87*, 5968.
(81) He, Z.; Cremer, D. *Theor. Chim. Acta* **1993**, *85*, 305.
(82) Roos, B. O. *Adv. Chem. Phys*. **1987**, *69*, 399. Ruedenberg, K.; Schmidt, M. W.; Gilbert M. M.; Elbert, S. T. *Chem. Phys. Lett*. **1984**, *109*, 212.
(83) Goldstein, E.; Beno, B.; Houk, K. N. *J. Am. Chem. Soc*. **1996**, *118*, 6036, and references therein.
(84) Bauschlicher, C. W., Jr.; Partridge, H. *J. Chem. Phys*. **1995**, *103*, 1788. Mebel, A. M.; Morokuma, K.; Lin, M. C. *J. Chem. Phys*. **1995**, *103*, 7414.